MODELING AMYOTROPHIC LATERAL SCLEROSIS WITH HUMAN IPSC-DERIVED MOTOR NEURONS ENGINEERED BY CRISPR/CAS9 GENOME EDITING TECHNOLOGY

by
Byung Woo Kim

A dissertation submitted to Johns Hopkins University in conformity with the requirements for

the degree of Doctor of Philosophy

Baltimore, Maryland
November 2020

Abstract

Amyotrophic lateral sclerosis (ALS) is a fatal neurodegenerative disorder characterized by the gradual degeneration and elimination of motor neurons (MNs) and denervation of skeletal muscles leading to paralysis, respiratory insufficiency, and death. Some familial ALS (fALS) is linked to mutations in the gene encoding copper, zinc superoxide dismutase 1 (SOD1). Its mutant forms are believed to acquire an adverse property. However, even with extensive in vivo animal modeling research on mutant SOD1, the true origin and onset of disease and underlying therapeutically relevant mechanisms on how the mutations in SOD1 cause neurodegeneration are unknown. An explanation for this failure can be found in attempts to translate experimental results that were derived from non-human animal models to clinical research for human disease treatment and on conceptual restrictions that the disease is only adult in its onset.

To compensate this limitation, human pluripotent stem cells (hPSCs), a promising source of vulnerable, disease-affected differentiated cells, have opened new prospects for understanding human tissue and organ development, disease modeling and mechanisms, and human disease-relevant therapeutic development and exploration. Here, we tested the hypothesis that hPSCs can provide novel insight into human ALS pathogenesis. Using human induced pluripotent stem cells (iPSCs) and the CRISPR/Cas9 genome editing system, we generated iPSCs carrying a G93A-SOD1 missense mutation. Using this mutant iPSC line, along with a patient-derived iPSC line with A4V-SOD1 mutation, we interrogated their directed differentiation into spinal motor neurons and identified neurodevelopmental and neurodegenerative defects when compared to isogenic wild-type neurons. The mutant MNs accumulated misfolded and aggregated forms of SOD1 in cell bodies and processes, including axons. They also developed distinctive axonal pathologies. Mutants had axonal swellings with shorter axon length and less numbers of branch

points. Moreover, structural and molecular abnormalities in presynaptic and postsynaptic size and density were found in the mutants. Our findings demonstrate that genome edited iPSC using CRISPR/Cas9-mediated targeted gene editing and their differentiation into motor neurons provide important tools to study mechanisms of disease in human ALS, including proteinopathy, axonopathy, and synaptic pathology. This work can provide needed new insight into human cell-relevant therapeutic targets.

Thesis Advisor: Lee J. Martin, Ph.D.

Thesis Readers: Lee J. Martin, Ph.D. and Phil Wong, Ph.D.

Acknowledgments

I thank my parents and brother who have been true advocates of me;

Friends who made my life in Baltimore fruitful;

My wife who has stood by me;

Committee members who have given me genuine support;

and Lee J. Martin who has always been there for me and encouraged me to never give up.

This work is supported by NIH-NINDS R01 grants NS034100 and NS052098, and NS065895.

Table of Contents

List of Tables

Page

List of Figures

Page

Chapter 1. Introduction

Amyotrophic lateral sclerosis (ALS) is a progressive neurodegenerative disorder characterized by the gradual degeneration and death of motor neurons. It is a fatal paralytic disease that causes muscle weakness, atrophy, paralysis, and ultimately, respiratory failure (Le Verche & Przedborski, 2010).

While mostly sporadic, about 10% of all ALS cases are familial which can provide a clue to vulnerability of motor neurons (Boylan, 2015). Certain familial cases of ALS are known to be associated with mutations in the superoxide dismutase 1 (SOD1) (Rosen et al., 1993), an antioxidant enzyme that is localized in the cytosol and other cellular compartments including nucleus and mitochondria. Acting as a homodimer, SOD1 binds to copper and zinc ions to destroy a toxic superoxide free radical (O_2^-) in the body (Petrov, Daura, & Zagrovic, 2016).

Despite its important physiological function, the mutant forms are thought to have crucial roles in the pathogenesis of the disease. It has been suggested in many studies that the mutations of SOD1 lead to destabilization of the protein structure and promote aggregation that are known to be selectively toxic to motor neurons. SOD1 knockout mice show distal axonopathy (Reaume et al., 1996), which may mimic early stages of ALS (Fischer et al., 2014), but they do not develop disease identical to ALS, suggesting toxic gain-of-function of mutant SOD1 might have more weight pathogenically than SOD1 loss of function in ALS (Munch & Bertolotti, 2010).

In order to understand how SOD1-mediated ALS initiates and propagate, researchers have been studying mutant SOD1 in different cell types using various models of ALS (Gurney et al., 1994; Wong et al., 1995). Jaarsma et al. specifically directed mutant SOD1 expression in neurons and showed induction of motor neuron degeneration and paralysis in Thy1.2-G93A transgenic mice (Jaarsma, Teuling, Haasdijk, De Zeeuw, & Hoogenraad, 2008). The experiment suggests a

motor neuron cell autonomous mechanism of disease. Another group showed that reducing the level of mutant SOD1-G37R within motor neurons slowed down the hindlimb weakness and axonal degeneration, also suggesting cell-autonomous contribution to ALS in disease onset and progression (Boillee et al., 2006). Non-cell autonomous components in ALS, which can selectively affect motor neurons, have also been widely studied. It has been shown in $SOD1^{G37R}$·$Olig^{-/-}$ chimeric mice that mutant SOD1 in cell types other than motor neurons and oligodendrocytes accelerated the disease onset (Yamanaka et al., 2008). *In vitro* co-culture of embryonic stem cell- or iPS cell-derived motor neurons and primary glial cells carrying SOD1-G93A mutation reduced motor neuron survival through toxic substance release, which additionally supports the role of non-motor neuronal population in ALS (Di Giorgio, Boulting, Bobrowicz, & Eggan, 2008).

Even with the extensive and intensive research on the protein and the disease over the past decades, little is known about the mechanisms of human SOD1 toxicity to motor neurons and there are no effective treatments available thus far to cure the disease (Kawamata & Manfredi, 2010). Riluzole and Edaravone are the two FDA-approved drugs for treating ALS but they may only extend lifespan of patients (Cruz, 2018; Fang et al., 2018).

A possible explanation for this shortcoming is the use of animal models that do not sufficiently replicate the human disease mechanisms. Many different disease models, including transgenic animals of ALS, have been used to understand pathogenesis and have contributed to a vast body of knowledge on pathobiology. Nevertheless, the outcome obtained from these models has not been translated into effective medical practices using disease-modifying therapies for ALS patients. The core of the problem may stem from the genetic variation between human and animals and differences in cell signaling and cell death mechanisms. In addition, overexpression

of mRNA or protein in some animal models and transfected cells make the models non-physiological, producing phenotypes that are contrary to those observed from ALS patients with a single copy of a mutant SOD1 gene (Ludolph et al., 2010; Morrice, Gregory-Evans, & Shaw, 2018; Philips & Rothstein, 2015).

Human induced pluripotent stem cells (iPSCs) are a promising source of differentiated cells and have recently opened new prospects for understanding human development, disease modeling and mechanisms, disease target identification, and therapeutic development. In particular, these cells can be obtained from both healthy and patient donors, making it possible for researchers to investigate human diseases in a physiopathological condition under the human genetic background. As a result, this model could complement existing models and potentially expedite clinical translation.

Here, we hypothesized that introduction of a disease-causing mutation, G93A-SOD1, to human iPSCs and their differentiation into spinal motor neurons will display spontaneously occurring ALS phenotypes and therefore, the cell line can be a valid and reliable disease model to study the disease. To test the hypothesis, we utilized CRISPR/Cas9 genome editing technology on iPSCs and introduced a SOD1-G93A missense mutation into the genome. By combining genome editing with stem cell differentiation approaches, we have generated highly pure spinal motor neuron lines that are “isogenic” to each other. With a patient-derived iPSC with A4V mutation as a positive control, we identified several disease phenotypes relevant to ALS. Misfolded and aggregated SOD1 were seen notably in the mutant motor neurons and its localization was not only confined to the soma but processes including the axon. Some axonal pathologies, including shorter axonal length, smaller number of branch points, and axonal swelling as well as soma attrition were observed in the mutants when compared to the wild-type.

As the cells were cultured longer and became more matured, smaller postsynaptic puncta sizes and lower synaptic puncta density were seen. Our findings suggest that iPSC-derived motor neurons combined with CRISPR/Cas9 genome editing technology can provide invaluable tools to promote in-depth study of ALS mechanisms of disease and disease target identification, and facilitate the application of scientific discoveries to clinical therapeutics.

Chapter 2. CRISPR/Cas9-mediated genome editing of human iPSC to generate fALS cell lines

Introduction

The advent of the CRISPR/Cas9 genome editing system in recent years has allowed us to create desired genetic modifications within cells and organisms with relatively improved targeting efficiency and precision. This system requires mainly two components; a guide RNA (gRNA) and a CRISPR-associated endonuclease (Cas9). With the help of the gRNA, which consists of a scaffold sequence needed for binding to Cas9 and a DNA targeting sequence that aims at the locus to be modified, the Cas9 endonuclease generates a site-specific double-stranded break in the genome where the genomic alteration occurs (Hsu, Lander, & Zhang, 2014; H. Li et al., 2020). Taking advantage of this reliable system, we hypothesized that CRISPR/Cas9 genome editing can introduce a disease-causing mutation, G93A, at *SOD1* gene locus by homology-dependent repair (HDR). Along with a single-stranded donor oligonucleotides (ssODN), which contains G93A-SOD1 mutation sequence, iPSCs were transfected with Cas9-gRNA ribonucleoprotein (RNP) by electroporation for CRISPR/Cas9-mediated HDR to generate an isogenic cell line. After single clone isolation and expansion, the genome-edited cells were validated and also tested for off-target effects. By this way, we obtained a reliable human cell model which expresses the mutant SOD1 at a physiological level.

Materials and Methods

iPSC culture: The institutional biosafety committee (JHU registration B1011021110) approved the use of human cells. The protocols met all ethical and safety standards for work on human cells. The human iPSC lines used in this study are identified in Table 1 and were characterized

previously (Y. Li et al., 2015; Wen et al., 2014). They were maintained on Matrigel-coated plates in StemFlex Medium (Gibco) and passaged every 4–6 days using EDTA or Accutase (Thermo Fisher Scientific).

Genome editing of human iPSCs by CRISPR/Cas9 system: Introduction of SOD1-G93A missense mutation by CRISPR/Cas9 genome editing technology was carried out using a healthy control iPSC line (C3-1). Prior to genome editing, alkaline phosphatase live staining (Invitrogen) was performed to verify pluripotency of iPSCs. Cells cultured on Matrigel (Corning) in StemFlex medium were pre-treated with Y-27632 ROCK inhibitor (Cellagen Technology) for 4–5 hr and dissociated with Accutase. Cells were resuspended with Cas9 nuclease (Invitrogen), guide RNA, and single-stranded DNA donor (Table 2) and electroporated (voltage of 1300V, pulse width of 10ms, 3 pulses) using Neon Transfection System (Invitrogen). After electroporation, cells were plated on Matrigel-coated plates and cultured for 48 hr. Cleavage efficiency was determined in a portion of the cells using GeneArt Genomic Cleavage Detection kit (Invitrogen). Remaining cells were passaged and cultured for 48–72 hr before performing clonal isolation. Single cells were isolated using Accutase and cultured for approximately 10–12 days. Each clonal cell line was collected and expanded. The genome editing of each clone was confirmed by DNA Sanger sequencing and digital droplet PCR. Genetic off-target effects were also analyzed.

Genetic off-target analysis: Potential off-target sites were analyzed by direct DNA sequencing. The top seven candidates were selected based on COSMID web tool (Cradick, Qiu, Lee, Fine, & Bao, 2014). Genomic DNA was isolated from iPSCs using DNeasy Blood & Tissue Kit (Qiagen). PCR amplification around the seven sites was performed and PCR products were sequenced. Primers used are listed in Table 3.

Alkaline phosphatase staining: An alkaline phosphatase live stain (Thermo Fisher Scientific) was used to identify undifferentiated, pluripotent iPSCs according to manufacturer's instruction. Briefly, iPSCs were washed twice with DMEM/F12 for 2-3 min. Alkaline phosphatase live stain was diluted at 1:500 in DMEM/F12 and cells were incubated for 20 min at 37 ℃. Cells were then washed twice with DMEM/F12 for 5 min. Following the wash, cells were imaged using Keyence BZ-X700 fluorescence microscope.

Digital droplet PCR: Detecting SOD1-G93A mutation in genome edited iPSCs and determining its copy number were done by performing digital droplet PCR (ddPCR). Reaction mix was first prepared by adding isolated genomic DNA, 1X ddPCR supermix, 1X target (FAM-labeled) and wild-type (HEX-labeled) primers/probe, MseI restriction enzyme, and H_2O. This was then loaded into DG8 cartridge along with droplet generation oil. The cartridge was placed in the QX200 droplet generator (Bio-Rad) for droplet generation. After the droplet was generated, they were transferred into a 96-well plate and thermal cycling was proceeded to amplify the sample. The plate containing the amplicons in droplets was subsequently placed and run in the QX200 Droplet Reader (Bio-Rad). Data analysis was done using the Quantasoft software (Bio-Rad) using at least 10,000 droplets.

Table 1. Human Induced Pluripotent Stem Cell Lines Used

iPSC lines (Clone)*	Gene	Mutation	Age of Donor	Gender
C3-1	Control	N/A	40	F
C3-1	SOD1	G93A	40	F
GO013	SOD1	A4V	63	F

*C3-1 and GO013 were provided by the Song lab (University of Pennsylvania) and the Rothstein lab (JHMI), respectively.

Table 2. List of Oligonucleotide Sequences

ID	Sequence (5'-3')	Purpose
SOD1-G93A-gRNA-fwd	TAATACGACTCACTATAGGAATCTTCAATAGACACA	gRNA DNA template for gRNA synthesis
SOD1-G93A-gRNA-rev	TTCTAGCTCTAAAACATGTGTCTATTGAAGATTC	
SOD1-G93A-ssODN	p-ZOCATCTGATGCTTTTTCATTATTAGGCATGTTGGAGACTTGGGCAATGTGACTGCTGACAAAGATGCTGTGGCAGATGTGTCTATTGAAGATTCZET	knock-in donor DNA
OT1-fwd	AGACACTGGCATTTCAGACGTAGG	Off-target analysis
OT1-rev	AGAAGACCCATGATTCCTGGGC	
OT2-fwd	CAAAGGTAGATCGCCAGAGACAAC	
OT2-rev	TGCCTGGTGGGAAGGTCCAT	
OT3-fwd	CAACCGGAGAAGTGACAAGGC	
OT3-rev	CTCAGATCAGTCTCTAGCAATCCC	
OT4-fwd	TCTGTAGTCAGCCTCTGTCCAC	
OT4-rev	CTTTCTGGGTCCCCAGTTTCTAC	
OT5-fwd	GGGCCTATGGAAGTGAACTCAAC	
OT5-rev	ATGTTGCATGTTTCTATGATGGGCCTATCC	
OT6-fwd	TCCTGGATGGTCCTGGACATCA	
OT6-rev	AGCAATGTGTGTCACTCCAGGATC	
OT7-fwd	GCAAATAAGCAACAGACCGAGGAG	
OT7-rev	GCCTCAGCTTTCTCATGTACCATC	

* p: 5'-phosphate, O: Phosphorothioate-C, E: Phosphorothioate-G, Z: Phosphorothioate-T

Results

Isogenic iPSC line with a SOD1-G93A missense mutation was generated by CRISPR/Cas9 genome editing.

To generate an isogenic iPSC line with a SOD1-G93A missense mutation, iPSC pluripotency was verified by alkaline phosphatase staining (Fig. 1C) prior to generating an isogenic iPSC line with a SOD1-G93A missense mutation. A guide RNA that specifically targets the wild-type allele and a single-stranded donor oligonucleotide were designed (Table 2), and together with Cas9 protein, they were delivered by electroporation into the cells to mediate genome editing (Fig. 1A and 1B). Single clones were isolated and expanded. Each clone was then frozen for stock and used for validation.

CRISPR gene edited cells were validated using Sanger sequencing, ddPCR, and off-target analysis.

Heterozygous *SOD1-G93A* mutation was confirmed by three methods; PCR amplification of the targeted region followed by direct DNA sequencing, droplet digital PCR, and off-target analysis. Sequencing the *SOD1* genomic locus showed that guanine was substituted by cytosine (GGT → GCT, ACC → AGC in reverse complementary strand) on one allele, resulting in the G93A mutation in the protein (Fig. 1D). We further detected and confirmed this heterozygous mutation by droplet digital PCR. Using two different fluorescent-labeled (FAM or HEX) probes that target either the mutant or the wild-type allele, ddPCR mutation detection assay was performed. As seen in the figure 1E, 1F, and 1G, the amount of wild-type template (HEX) and that of the mutant template (FAM) were comparable, demonstrating the G93A mutation in one allele. After confirming the site-specific mutation, seven potential off-target sites were examined and we confirmed that no off-target mutations were induced by CRISPR (Table 3).

Figure 1. Establishment of SOD1$^{+/G93A}$ iPSC.

(A) CRISPR/Cas9 genome editing workflow. (B) Schematic representation of CRISPR/Cas9-mediated genome editing. The PAM sequence and the mutation site are shown in red and blue, respectively. (C) Phase-contrast image of human iPSCs and alkaline phosphatase live staining showing stem cell pluripotency. Scale bar, 50 μm. (D) Chromatogram demonstrating CRISPR/Cas9-mediated genome editing of SOD1$^{+/+}$ to SOD1$^{+/G93A}$. The sequence of a reverse complementary strand is shown. (E) Two-dimensional ddPCR scatter plot showing the four droplet clusters identified with a mutant and wild-type allele; FAM/HEX negative (grey), FAM positive (blue), HEX positive (green), and FAM/HEX positive (orange). (F-G) Concentrations and ratio of mutant and wild-type allele.

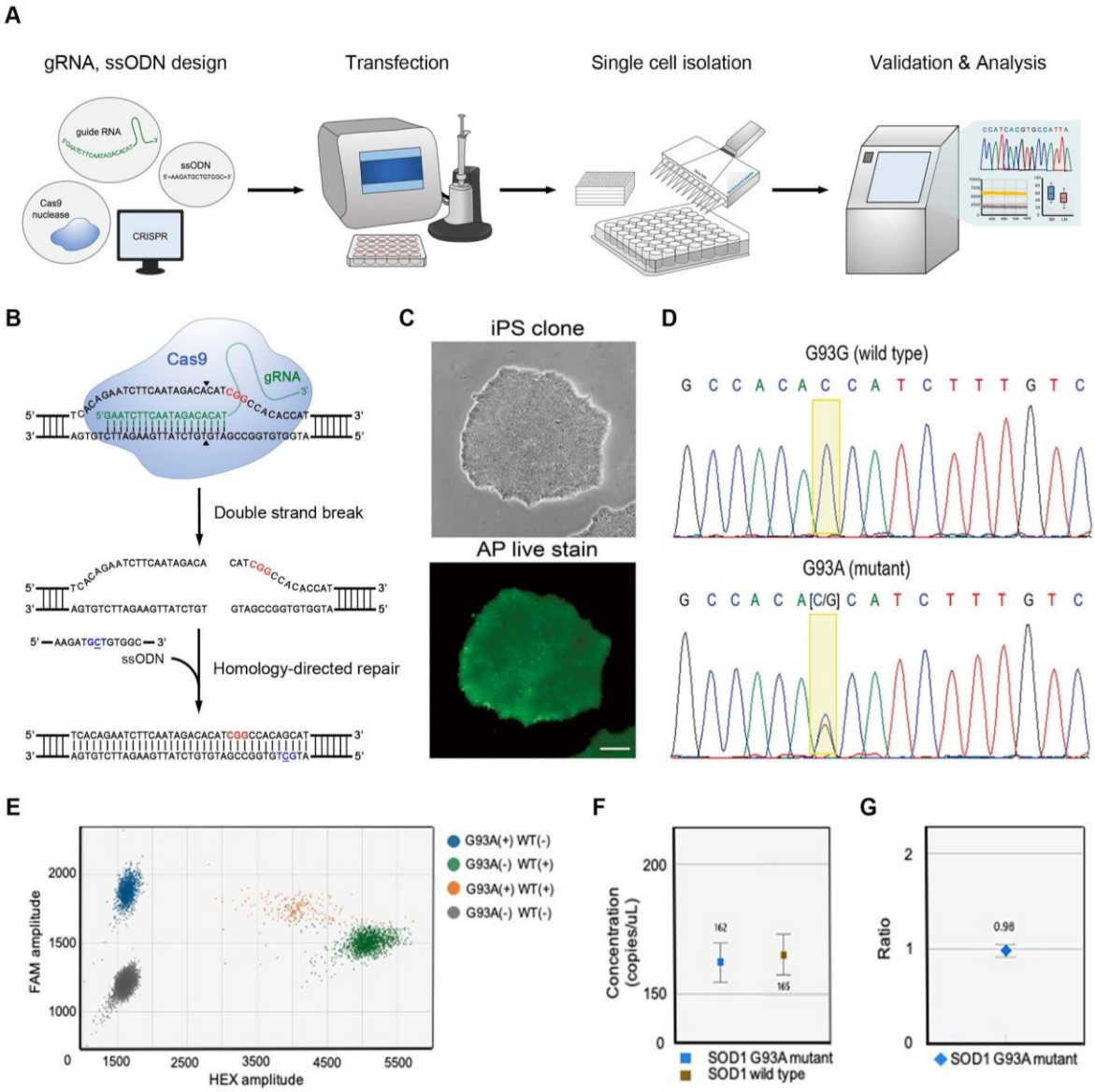
A
gRNA, ssODN design
Transfection
Single cell isolation
Validation & Analysis
guide RNA
ssODN
Cas9 nuclease
CRISPR
B
Cas9
gRNA
Double strand break
ssODN
Homology-directed repair
C
iPS clone
AP live stain
D
G93G (wild type)
G C C A C A C C A T C T T T G T C
G93A (mutant)
G C C A C A [C/G] C A T C T T T G T C
E
G93A(+) WT(-)
G93A(-) WT(+)
G93A(+) WT(+)
G93A(-) WT(-)
FAM amplitude
HEX amplitude
F
Concentration (copies/uL)
162
165
SOD1 G93A mutant
SOD1 wild type
G
Ratio
0.98
SOD1 G93A mutant

Table 3. Summary of Off-Target Analysis*

ID	Sequence	Mismatch	Score	Chromosome position	Mutation
OT1	**C**AA**AA**TTCAATAGACACATG GG -- hit GAATCTTCAATAGACACATN GG – query	3	0.53	Chr15:25520090 -25,520,111	Not detected
OT2	G**T**AT**A**TTC**C**ATAGACACATG GG -- hit GAATCTTCAATAGACACATN GG – query	3	0.86	Chr4:109681139 -109,681,160	Not detected
OT3	**TC**ATCTTCAA**A**AGACACATT GG -- hit GAATCTTCAATAGACACATN GG – query	3	1.08	Chr13:46227046 -46,227,067	Not detected
OT4	G**T**ATCTT**G**AA**A**AGACACATG GG -- hit GAATCTTCAATAGACACATN GG – query	3	1.3	Chr11:87945053 -87,945,074	Not detected
OT5	GA**T**TCT**A**CAAT**G**GACACATT GG -- hit GAATCTTCAATAGACACATN GG – query	3	1.54	Chr12:24874767 -24,874,788	Not detected
OT6	GAAT**T**T**C**CAAT**G**GACACATT GG -- hit GAATCTTCAATAGACACATN GG – query	3	1.58	Chr7:134494940 -134,494,961	Not detected
OT7	**A**AATCTT**T**AATA**C**ACACATC GG -- hit GAATCTTCAATAGACACATN GG – query	3	1.78	Chr4:107649971 -107,649,992	Not detected

*Mismatched bases are in bold

Discussion

Generation of human iPSCs harboring G93A missense mutation using CRISPR/Cas9 genome editing system has provided an unprecedented tool that expresses mutant G93A-SOD1 at physiological level under human genetic background with minimized variation. This cell line is novel and particularly important since G93A mutation in ALS is one of the most common forms and intensively studied, especially in mice, yet it has never been introduced in iPSCs before. This can be a great addition to the iPSC-based ALS research along with other available iPSC lines with SOD1 mutations including A4V, D90A, R115G, E100G, N87S, S106L, A272C, L144FVX, N139K, V148G, and L144F (Amoroso et al., 2013; Bhinge, Namboori, Zhang, VanDongen, & Stanton, 2017; Chestkov, Vasilieva, Illarioshkin, Lagarkova, & Kiselev, 2014; Imamura et al., 2017; Naujock et al., 2016; Richard & Maragakis, 2015; Seminary, Sison, & Ebert, 2018; L. Wang et al., 2017).

Experimental design of CRISPR/Cas9 components was critical in acquiring high efficiency in homology directed repair (HDR), yielding precise editing. First, the protospacer adjacent motif (PAM) sequence, 2-6 base pair DNA sequence of 5'-NGG-3' where N is any nucleotide base, is required near the intended edit site. Without the PAM sequence, Cas9 nuclease cannot successfully bind and cleave the target DNA sequence. Having a PAM sequence in proximity to the edit site will result in double-stranded break (DSB) just a few additional bases up or downstream from the target locus, which in turn enhances the editing efficiency. The dose of ssODN was another crucial element and affects the HDR frequencies. The asymmetric, single-stranded DNA donor with the optimal concentration of 1200 nM improved efficiency (11.1% knockin efficiency) when compared to the ssODN concentration of 800 nM. Previous studies have shown that the length of ssODN also affects the result as the use of shorter or longer

oligonucleotides tends to increase the incidence of errors (Liang, Potter, Kumar, Ravinder, & Chesnut, 2017).

Some shortcomings of the CRISPR/Cas9 system do exist and need improvements in order to make it more efficient and applicable in medical practices. As already mentioned, the system is dictated by the availability of the PAM sequence near the edit site. For targeted loci without PAM sequence nearby, DSB will not occur in close proximity to the loci, resulting in low editing efficiency (Liang et al., 2017). Besides, DSB induced by Cas9 nuclease could be dangerous because unintended genetic modifications can be made after the cut. Together with possible off-targets, it can result in unpredicted side effects including genetic damage and extensive mutations throughout the genome (Kosicki, Tomberg, & Bradley, 2018). Also, the current system *in vitro* relies on the cell types that are capable of cell division, meaning that non-dividing, postmitotic cells, such as neurons, are not feasible (Tan, Huang, & Ngeow, 2018). With some optimizations and refinements of the system that can overcome these drawbacks, CRISPR/Cas9 genome editing technique can be a more robust and powerful tool.

The acquisition of an iPS cell line with an SOD1 mutation, G93A, supports the needs for revealing naturally occurring pathology and ultimately elucidating the mechanisms of ALS for therapeutics. In addition, combining differentiation protocols for ALS-relevant cell types, including motor neurons and muscle cells, could provide better understanding of the disease. For example, co-culture of ALS motor neurons with skeletal muscle will form neuromuscular junctions (NMJs), which are one of the first sites affected in ALS, and mimic the in vivo disease environment in human cultures (Ionescu & Perlson, 2019). Together with cell differentiation and in vitro multicellular co-culture approaches, the genome-edited isogenic line can possibly

provide the true ALS disease phenotypes as seen in human ALS tissues and possibly distinct from those seen in animal models.

Chapter 3. Differentiation of human iPSCs into highly pure spinal motor neuron cultures

Introduction

ALS is a motor neuron disease. It is characterized by gradual deterioration and death of both upper and lower motor neurons with lower or spinal motor neurons being anatomically and pathologically affected earlier as evidenced by damage in the neuromuscular junctions (Moloney, de Winter, & Verhaagen, 2014; Murray, Talbot, & Gillingwater, 2010). In an effort to effectively understand the primary cause of the disease, we used iPSCs harboring SOD1 mutations, including a line created by CRISPR/Cas9, and hypothesized that the iPSCs can be differentiated into highly pure spinal motor neurons for their interrogation in cell culture. Using the principles of embryogenesis and small molecule morphogens, more than 80% of the cell population were differentiated into mature motor neurons within 28 days. These iPSC-derived motor neurons were not only morphologically and immunophenotypically motor neurons but they were also functionally active.

Materials and Methods

Cell culture: iPSC cell culture is described in chapter 2. For mouse embryonic fibroblasts (MEFs), we used CF-1 mouse embryos at approximately 13.5 days gestation. MEFs were cultured in Dulbecco's modified Eagle's medium (DMEM, Corning) supplemented with 10% fetal bovine serum (FBS, Hyclone), 1% Minimum Essential Medium Non-Essential Amino Acids (MEM-NEAA, Gibco), and 1% GlutaMAX (Gibco). Mouse cortical astrocytes, which were used for patch clamp recording and to enhance attachment of motor neurons, were isolated

from 3 to 4 postnatal day old CD1 mouse pups as described (Schildge, Bohrer, Beck, & Schachtrup, 2013) and cultured in DMEM supplemented with 10% FBS.

Differentiation of human iPSCs into motor neurons: Generation of iPSC-derived spinal motor neurons was done using published protocols (Calder et al., 2015; Du et al., 2015; Maury et al., 2015) with some modifications developed in this work (Fig. 2). In brief, iPSCs were passaged onto MEF feeder layers in DMEM/F12 culture medium supplemented with 20% KnockOut Serum Replacement (Gibco), 1% MEM-NEAA, 1% GlutaMAX, 10 ng/mL bFGF (PeproTech), 0.1 mM β-mercaptoethanol (Gibco), and 10 μM Y-27632 ROCK inhibitor. On the next day, the medium was changed to modified N2/B27 medium (DMEM/F12:Neurobasal [1:1], 0.5% N2, 0.5% B27, 0.1 mM ascorbic acid, and 1% GlutaMAX) containing 3 μM CHIR-99021 (Tocris), a glycogen synthase kinase-3 inhibitor, along with the combination of 2 μM SB-431532 (Tocris), a transforming growth factor-β receptor inhibitor, and 2 μM DMH-1 (Tocris), a bone morphogenic protein type I receptor/activin receptor-like kinase-2 (ALK2) inhibitor. iPSCs were cultured in this condition for 6–7 days. The cell clusters were detached with 0.1% (w/v) collagenase IV (Gibco) and plated on Matrigel-coated plates in the same medium supplemented with 1 μM CHIR-99021, 2 μM SB-431532, 2 μM DMH-1, 0.1 μM retinoic acid (RA, Sigma), and 0.5 μM purmorphamine (Stemgent), a hedgehog agonist. After maintaining cell clusters for 6–7 days, they were collected by collagenase IV and further differentiated in ultra-low attachment plates (Corning) containing modified N2/B27 medium with 0.5 μM RA and 0.1 μM purmorphamine (PUR) and grown in suspension for another 6–7 days. Cell clusters were then singlized with Accutase and plated on Matrigel-coated plates or on mouse primary astrocytes for additional 10 days with 0.5 μM RA, 0.1 μM PUR, 0.1 μM Compound E (Millipore), a Notch pathway inhibitor, and three neurotrophic factors (PeproTech): 10 ng/ml brain-derived neurotrophic factor

(BDNF); 10 ng/ml ciliary neurotrophic factor (CNTF); and 10 ng/ml insulin-like growth factor 1 (IGF-1). We also utilized alternative cell culture conditions. For neural patterning, 10 μM SB-431532 and 200 nM LDN-193189 (Stemgent), an ALK2/3 receptor inhibitor, was used. For motor neuron specification, a combination of 10 μM SB-431532 and 200 nM LDN-193189 was used as a substitute for 1 μM CHIR-99021, 2 μM SB-431532, and 2 μM DMH-1. Lastly, for motor neuron differentiation, we sometimes used 0.5 μM RA, 0.1 μM purmorphamine, 5 μM DAPT (Stemgent), a γ-secretase inhibitor, with BDNF, CNTF, and IGF-1. In all instances, neuronal cultures were treated with 50 μm 5-Fluoro-2'-deoxyuridine (Sigma) on the following day of plating for 24 hr to inhibit proliferation of any undifferentiated progenitor cells or astrocytes. All culture media in each stage were changed every 2 days. Cells in each stage were immunophenotyped using appropriate antibodies.

Immunofluorescence staining: Cells on glass coverslips were fixed in 4% paraformaldehyde for 10 min at room temperature and washed three times with PBS. Fixed cells were first permeabilized with 0.2% Triton X-100 in PBS for 10 min and were subsequently blocked in PBS with 10% donkey serum for 1 hr. Following blocking, cells were incubated overnight at 4 °C with primary antibodies diluted in blocking solution. The following primary antibodies were used: goat polyclonal anti-SOX1 (1:50, R&D systems), mouse monoclonal anti-OTX2 (1:100, DSHB), rabbit polyclonal anti-HOXA3 (1:100, Sigma), rabbit polyclonal anti-OLIG2 (1:500, Millipore), mouse monoclonal anti-NKX2.2 (1:100, DSHB), mouse monoclonal anti-ISL (1:100, clone 40.2D6, Developmental Studies Hybridoma Bank [DSHB]), mouse monoclonal anti-Hb9 (1:50, clone 81.5C10, DSHB), goat polyclonal anti-choline acetyltransferase (ChAT, 1:100, Millipore), chicken polyclonal anti-microtubule–associated protein-2 (MAP 2, 1:5000, Novus Biologicals), mouse monoclonal anti-TUJ1 (1:2000, clone 5G8, Promega), rabbit polyclonal

anti-TUJ1 (1:3000, Covance), mouse monoclonal anti-synaptophysin (SYPH, 1:300, clone EP10, Invitrogen), and mouse monoclonal anti-PSD95 (1:200, clone K28/43, NeuroMab). Non-immune IgG isotypes were used as negative controls at concentrations identical to the primary antibodies. After antibody incubations, cells were rinsed in PBS, incubated with secondary antibodies (Alexa-Fluor-488, Alexa-Fluor-594, and Alexa-Fluor-647, Thermo Fisher Scientific) diluted at 1:500, rinsed in PBS, and then stained with Hoechst 33258 DNA dye for nuclear visualization.

Neuromuscular junction formation: Rat L6 myoblasts were seeded on matrigel-coated coverslips in a 24-well plate and grown in DMEM supplemented with 10% FBS. The medium was replaced by DMEM with 2% horse serum at 60-70% confluency to induce myotube differentiation. iPSC-derived motor neurons were then added to the plate with medium replaced by modified N2/B27 medium containing 0.5 μM RA, 0.1 μM PUR, 0.1 μM Compound E, and three neurotrophic factors: 10 ng/ml brain-derived neurotrophic factor (BDNF); 10 ng/ml ciliary neurotrophic factor (CNTF); and 10 ng/ml insulin-like growth factor 1 (IGF-1). The cells were cocultured for additional 7-10 days and were visualized using α-bungarotoxin (α-BTX) and ChAT staining.

Electrophysiological characterization by whole-cell patch clamp recording: DIV 28 differentiated motor neuron culture on round coverslips (12-mm diameter) were put into a submersion recording chamber on an upright microscope (Zeiss AxioExaminer, Objectives: 5x, 0.16 NA and 40x, 1.0 NA) fitted for infrared differential interference contrast (IR-DIC). The recording chamber was continuously superfused (2-4 ml/min) with artificial cerebrospinal fluid (aCSF) composed of (in mM): 125 NaCl, 26 $NaHCO_3$, 2.5 KCl, 1.25 NaH_2PO_4, 1 $MgSO_4$, 20 glucose, 2 $CaCl_2$, 0.4 ascorbic acid, 2 pyruvic acid, and 4 L-(+)-lactic acid; pH 7.3, 315 mOsm, continuously bubbled with 95% O_2/5% CO_2. Neurons were visualized with a digital camera (Sensicam QE; Cooke). Glass recording electrodes (2-4 MΩ) were filled with an internal

solution containing (in mM): 2.7 KCl, 120 KMeSO4, 9 HEPES, 0.18 EGTA, 4 MgATP, 0.3 NaGTP, 20 phosphocreatine (Na), pH 7.3, 295 mOsm. Cell electrical activities were obtained by using a Multiclamp 700B amplifier (Molecular Devices) and an ITC-18 (Instrutech), both controlled by using a customized routine written by Igor Pro (Wavemetrics). 1-sec-long 10-100 pA currents were injected into the cells to evoke action potentials and -20 pA currents were injected to investigate hyperpolarizing responses of the cells. In a subset of current-step test, cells membranes were held at ~80 mV to see action potential initiation more clearly. All signals were low-pass filtered at 10 kHz and sampled at 20 kHz.

Microscopy and image acquisition: Cells on coverslips were mounted in ProLong Gold Antifade Mountant (Thermo Fisher Scientific, P36930) and confocal images were taken and analyzed using Leica TCS SP8 microscope and LAS X software (Leica, Germany).

Results

Highly pure human spinal motor neuron cultures were generated from iPSCs.

Using this genome-edited SOD1-G93A iPSC line along with its isogenic control wild-type and patient-derived SOD1-A4V iPSC lines, we differentiated cells into highly pure spinal motor neurons, as confirmed by motor neuron markers. We first promoted neural induction using iPSCs to generate neural progenitor cells (NPCs). From immunofluorescence staining, we showed that nearly all the cells after 6-7 days of differentiation were SOX1, which is a marker for NPCs. Also, we confirmed that those SOX1-positive cells were HOXA3 positive but OTX2 negative, demonstrating that the cells were of caudal fate, not rostral (Fig. 2C). Ventralization of NPCs were undergone for the following 6-7 days and motor neuron progenitors (MNPs) were identified by OLIG2. NKX2.2, which is another ventral spinal cord marker but mainly used for identifying interneuron progenitor, was used along with OLIG2 and showed that its expression

was completely repressed (Fig. 2D). The cells were further differentiated in suspension culture as spheroids for another 6-7 days. At 18–21 days of differentiation, greater than 80% of the cells were ISL1 and Hb9 positive (Fig. 2E and 2G). Approximately 80–90% of the cells were positive for ChAT, a mature motor neuron marker, and showed multipolar morphology at 28–31 days of differentiation (Fig. 2E and 2H).

iPSC-derived human motor neurons show synaptic maturation.

The iPSC-derived motor neurons were also positive for SYPH and PSD95, a presynaptic and a postsynaptic marker. With the average size of presynaptic puncta being generally larger than that of postsynaptic puncta, both $SYPH^+$ presynaptic puncta and $PSD95^+$ postsynaptic puncta became more prominent in sizes and numbers over time (Fig. 2F and 2I), indicating maturation of synapses in the motor neuron culture.

iPSC-derived human motor neurons are functionally active.

To determine whether the motor neurons are electrophysiologically functional to fire action potential, we performed whole cell patch-clamp recordings. As shown in Fig. 3B, the neurons fired functional action potentials in response to depolarizing current step injections, and displayed hyperpolarization followed by post-rebound action potential in response to negative current injections (Fig. 3C). We also checked whether these cells can form NMJs when co-cultured with rat L6 myotubes. After 7-10 days of co-culture, we observed α-BTX bound to acetylcholine receptors, overlapped with ChAT-positive neurites, indicating the formation of NMJs (Fig. 3D). These data show that the motor neurons are not only having multipolar morphology and expressing motor neuron markers, but they also are functionally active.

Figure 2. Differentiation of iPSCs into spinal motor neurons using small molecules.

(A) Schematic diagram showing the protocol used for motor neuron differentiation from iPSCs. (B) Phase-contrast images of cell types in each differentiation stage. Scale bar, 200 μm and 25 μm. (C) Immunofluorescence image of $SOX1^+$ and $OTX2^-$ NEPs after 6 days of culture. Scale bar, 50 μm. (D) Immunofluorescence image of $OLIG2^+$ MNPs on day 12. (E) Representative images of $ISL1^+$, $Hb9^+$, and $ChAT^+$ MNs on day 28. (F) Representative images of $SYPH^+$ and $PSD95^+$ MNs on day 60. Scale bar, 20 μm. (G and H) Quantification of $ISL1^+$, $Hb9^+$, and $ChAT^+$ MNs on (G) day 18 and (H) 28. (I) Quantification of $SYPH^+$ and $PSD95^+$ MNs on day 30 and 60. All data shown as means ± SEM.

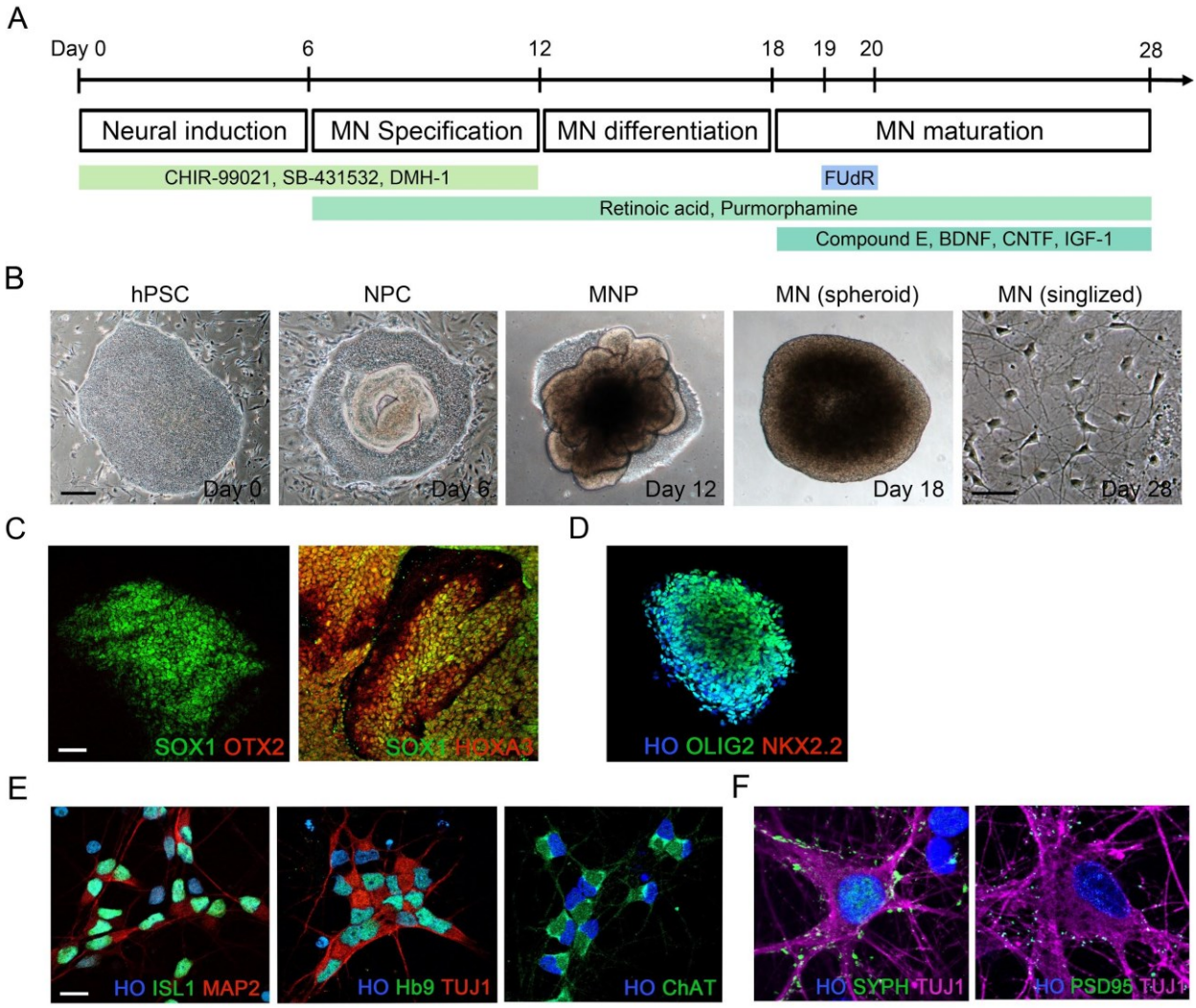

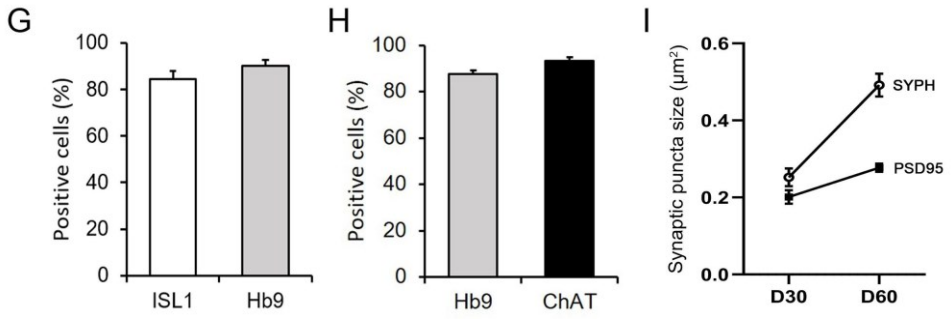

Figure 3. Functional analysis of iPSC-derived motor neurons

(A) Whole cell patch-clamp recording on a motor neuron on day 28. Scale bar, 50 μm. (B) Induced high frequency action potential bursts. (C) Hyperpolarization induced rebound action potentials. (D) NMJ formation in co-culture with L6 rat myotubes. Scale bar, 50 μm.

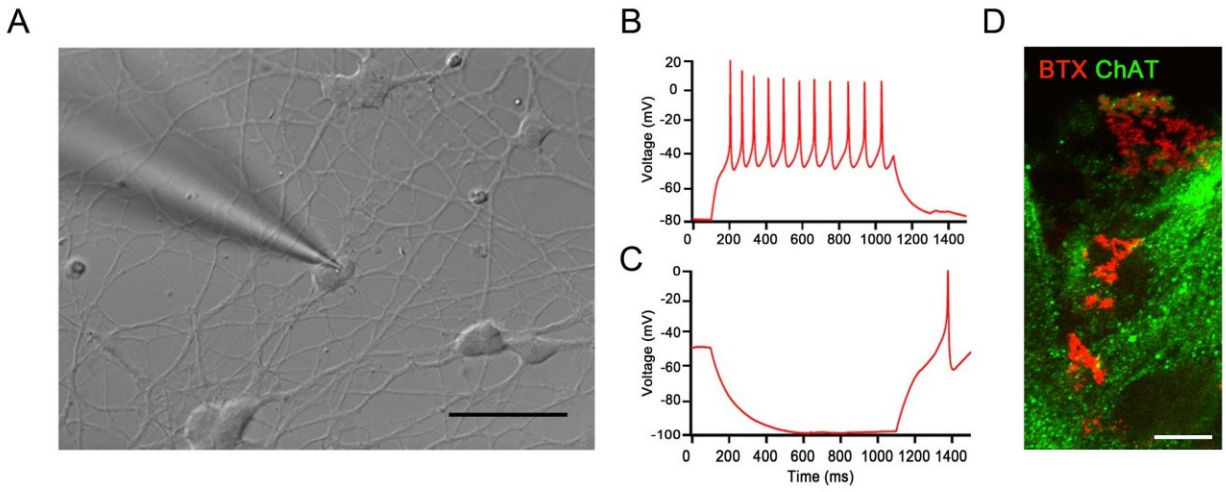

Discussion

Although the emergence of iPSCs have undeniably opened new avenues for biomedical research, modeling diseases with iPSCs has been experiencing various technical challenges such as heterogeneous cell population including unwanted cell types and poorly differentiated immature cells, and genetic differences between individuals (Chen et al., 2014). In ALS studies, for example, having motor neurons and glia bearing the same ALS mutation in a dish could hinder researchers from knowing pathophysiology of the disease including the autonomy of cell

degeneration. Furthermore, even with the pure motor neurons and the same ALS mutation, the extent of genetic variation among different iPSC lines could also be an important factor to consider because it can skew the experimental results (Burrows et al., 2016; Guhr et al., 2018; Vigilante et al., 2019).

Using the principles of embryogenesis and small molecule morphogens, we have generated highly pure spinal motor neurons which liberated us from confounders of cell heterogeneity and thus, identified disease phenotypes will be in the cell type of interest, rather than in a non-motor neuron population. WNT-activation/dual SMAD inhibition-based method was used by adding a WNT agonist, CHIR-99021, and two SMAD inhibitors, SB-431532 and DMH-1, to iPSC culture as activating WNT signaling and inhibition of SMAD signaling have been shown to efficiently promote neural induction. WNT signaling has also been demonstrated to be vital in determining ventral spinal cord cell fates. As RA induces caudal neuronal subtypes and SHH is involved in ventralization in the spinal cord, exposure of RA and PUR, a SHH agonist, to NPCs resulted in motor neuron specification and differentiation. Inhibition of NOTCH signaling by a γ-secretase inhibitor, compound E or DAPT, and supplementing neurotrophic factors to motor neurons further matured the cells. By day 28, we could obtain a very pure motor neuron population, between 80-90% of the total population, as confirmed by ISL1, Hb9, and ChAT. The rest of the non-motor neuron cell population, which includes undesired cell types and/or poorly differentiated cells, was prevented from further proliferation by addition of a mitotic inhibitor, 5-Fluoro-2'-deoxyuridine (FUDR). Together with CRISPR/Cas9 genome editing technology, which allowed us to perform knockin of G93A-SOD1 mutation within the human genome of iPSCs, generation of an isogenic mutant motor neurons will become an invaluable tool for disease modeling and ultimately for elucidating disease mechanisms and therapeutics.

Chapter 4. Disease phenotypes of fALS in genome-edited iPSC-derived motor neurons

Introduction

Modeling ALS by combining human iPSC-derived motor neurons with SOD1 mutations and CRISPR/Cas9 genome editing is an advantageous and appropriate approach to understand various cellular and molecular aspects of the disease while carefully controlling genetic background and maintaining physiological condition. Here, we hypothesized that genome edited iPSC-derived motor neurons with SOD1-G93A mutation show human ALS-relevant disease phenotypes and therefore, can be a proper model to study the disease. A healthy control iPSC line (C3-1) and a patient-derived SOD1-A4V line (GO013) were also differentiated into motor neurons and used as an isogenic and a disease positive control, respectively. By using these strategies, we found that mutant motor neurons showed markedly increased misfolded and aggregated SOD1 in their cell bodies and processes. Axonopathy, which is defined as functional and structural degradations in the axon, were also observed in the mutants when compared to the wildtype. Furthermore, we observed some signs of synaptic dysregulations which could impact the degeneration and death of ALS motor neurons.

Materials and Methods

Extraction of misfolded and aggregated SOD1 in motor neuron cell lysates: Approximately 6 x 10^6 motor neurons for each line were used. Cells were first washed with PBS and harvested by centrifugation for 5 min at 200 g, 4°C. RIPA buffer with protease inhibitor was added to the pellet and the cells were incubated for 20 min on ice. During the incubation, probe sonication was performed briefly for 2-3 times to disrupt cell membranes and homogenize the samples. The

lysates were centrifuged for 10 min at 14,000 g, 4 ℃ and the supernatant (RIPA-soluble fraction) was collected. The pellet was washed with PBS and centrifuged again with the same condition. UREA buffer (8 M UREA, 4% CHAPS, 40 mM Tris, 0.2% BioLyte 3/10 ampholyte, 2 mM tributylphosphine) with protease inhibitor was then added to the pellet. After incubation for 30 min at room temperature, the samples were centrifuged for 10 min at 14,000 g, 4 ℃ and supernatant (UREA-soluble fraction) was collected.

Western blotting of RIPA- and UREA-soluble fractions: Protein concentrations were determined by Pierce BCA Protein Assay Kit (Thermo Fisher Scientific). 25 μg of proteins from RIPA-soluble fractions and equivalent volumes of proteins from UREA-soluble fractions were loaded and separated by SDS-PAGE. Samples were transferred onto nitrocellulose membranes, washed with a blocking buffer, and probed with rabbit polyclonal anti-SOD1 (1:5000, abcam) overnight at 4 ℃. The membrane was washed three times in the blocking buffer for 5min and probed with secondary antibody conjugated with HRP (1:10,000, Invitrogen) for 1 hr. Bands were detected with Pierce ECL western blotting substrate (Thermo Fisher Scientific).

Cell body size, axon length, and branch point measurement: Motor neuron spheroids on day 18 were dispersed into single cells, plated on coverslips in 24 well plates, and grown for additional 2, 4, and 6 days. Cells were fixed with 4% paraformaldehyde at each time point and immunostained with neuronal markers including TUJ1, MAP2, and Tau. Cell body sizes of motor neurons of each cell line at 4 days after plating were measured using ImageJ. For axon length measurement, an axon of a cell was first identified by a neurite that is Tau-positive but MAP2-negative. Using ImageJ, the length of the neurite was quantified. Only those neurons with axons that had more than twice the length of cell body were selected and measured. To count the number of branch points of both dendrites and axons, tracings of individual cells were first

performed. This was done semi-automatically by using the NeuronJ plugin of ImageJ with fluorescence images taken 4 days after plating.

Quantification of synapse size and density: Motor neurons on day 60 were fixed and immunostained with the following antibodies; rabbit polyclonal anti-synapsin (1:500, Synaptic systems) and mouse monoclonal anti-PSD95 (1:200, clone K28/43, NeuroMab). Fluorescence images of motor neurons were taken and analyzed using ImageJ: The area of each puncta was measured for quantifying synapse size. Images used for analyses were thresholded with a constant value for each channel. For synaptic density, the number of puncta per 100 μm was measured using a plugin Puncta Analyzer.

Statistical analysis: Statistical analyses were performed by using one-way analysis of variance using GraphPad Prism, version 8. All data are represented as mean ± SEM. Statistical significance was considered when p-value was less than 0.05.

Results

Increased level of misfolded and aggregated SOD1 was observed in $SOD1^{+/G93A}$ and $SOD1^{+/A4V}$ motor neurons under basal culture conditions.

SOD1 with missense mutations associated with familial ALS is known to be more prone to misfolding and aggregation (Elam et al., 2003; Johnston, Dalton, Gurney, & Kopito, 2000; Shinder, Lacourse, Minotti, & Durham, 2001; J. Wang, Xu, & Borchelt, 2002). Although controversial, misfolded SOD1 has also been studied and described as a pathological feature found in sporadic ALS (Kabashi, Valdmanis, Dion, & Rouleau, 2007; Rotunno & Bosco, 2013). Using the pair of isogenic iPSC lines along with a patient-derived iPSC line with A4V-SOD1 mutation, we examined the presence of misfolded and aggregated SOD1 in differentiated motor

neurons under basal culture condition. As shown in figure 4A and 4C, immunofluorescence results showed that approximately 20-25% of motor neurons with either A4V-SOD1 or G93A-SOD1 mutation were positive for a well-characterized misfolded SOD1 antibodies, C4F6. In addition, some of those motor neurons with the reactivity had inclusions (Fig 4B and 4D). Motor neurons with wild-type SOD1 also showed a low level of reactivity and inclusions, perhaps representing basal endogenous misfolding of wildtype SOD1. These results were also confirmed by immunoblotting assays on RIPA detergent soluble and insoluble fractions obtained from the motor neuron culture. Compared to the wild-type SOD1 motor neuron culture, the amount of detergent insoluble SOD1 in the UREA soluble fractions of $SOD1^{+/G93A}$ and $SOD1^{+/A4V}$ motor neurons was notable (Fig. 4F and 4G). Moreover, when looking at the localization of misfolded SOD1, the protein was not only present in the cell body but also in the processes including dendrites and axons (Fig. 4H)

Figure 4. SOD1 Misfolding and aggregation in motor neuron cultures.

(A) Immunofluorescence images of motor neurons showing C4F6 immunoreactivity, an indicative of misfolded SOD1. Scale bar, 20 μm. (B) Quantification of C4F6 and B8H10-positive cells. (C) Experimental procedures of extracting RIPA-soluble and UREA-soluble fractions from motor neuron cultures. (D) Western blots showing SOD1 in RIPA-soluble and UREA-soluble fractions. GAPDH was used as a loading control. (E) Immunofluorescence image of motor neurons showing C4F6-positive inclusions. (F) Quantification of cells with C4F6 inclusions. (G) Immunofluorescence images of motor neurons showing the localization of misfolded SOD1. Scale bar, 10μm. All data shown as means ± SEM. (B and F) n = minimum of 266 cells per well with a total of 949 cells with $SOD1^{+/A4V}$ mutation, 876 cells with $SOD1^{+/G93A}$ mutation, and 1072 cells with $SOD1^{+/+}$ from 3 wells for each line. $*p < 0.05$, $**p < 0.01$.

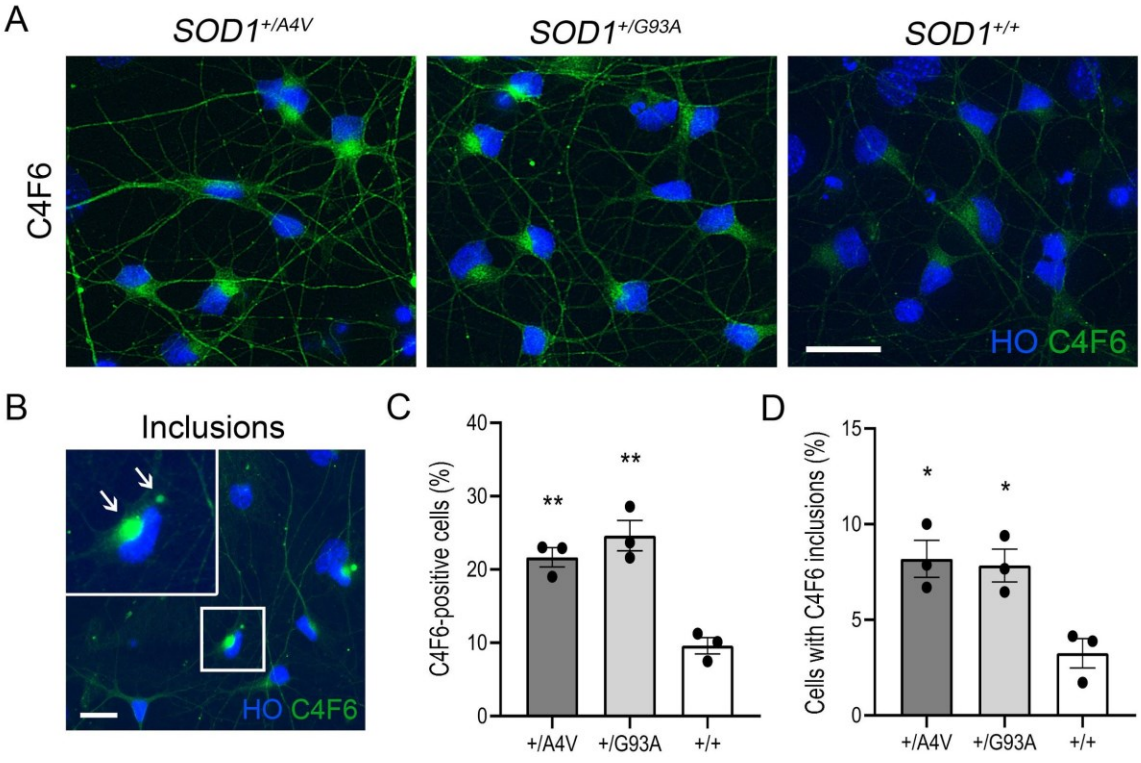
A
SOD1+/A4V
SOD1+/G93A
SOD1+/+
C4F6
HO C4F6
B
Inclusions
HO C4F6
C
C4F6-positive cells (%)
40
30
20
10
0
**
**
+/A4V
+/G93A
+/+
D
Cells with C4F6 inclusions (%)
15
10
5
0
*
*
+/A4V
+/G93A
+/+

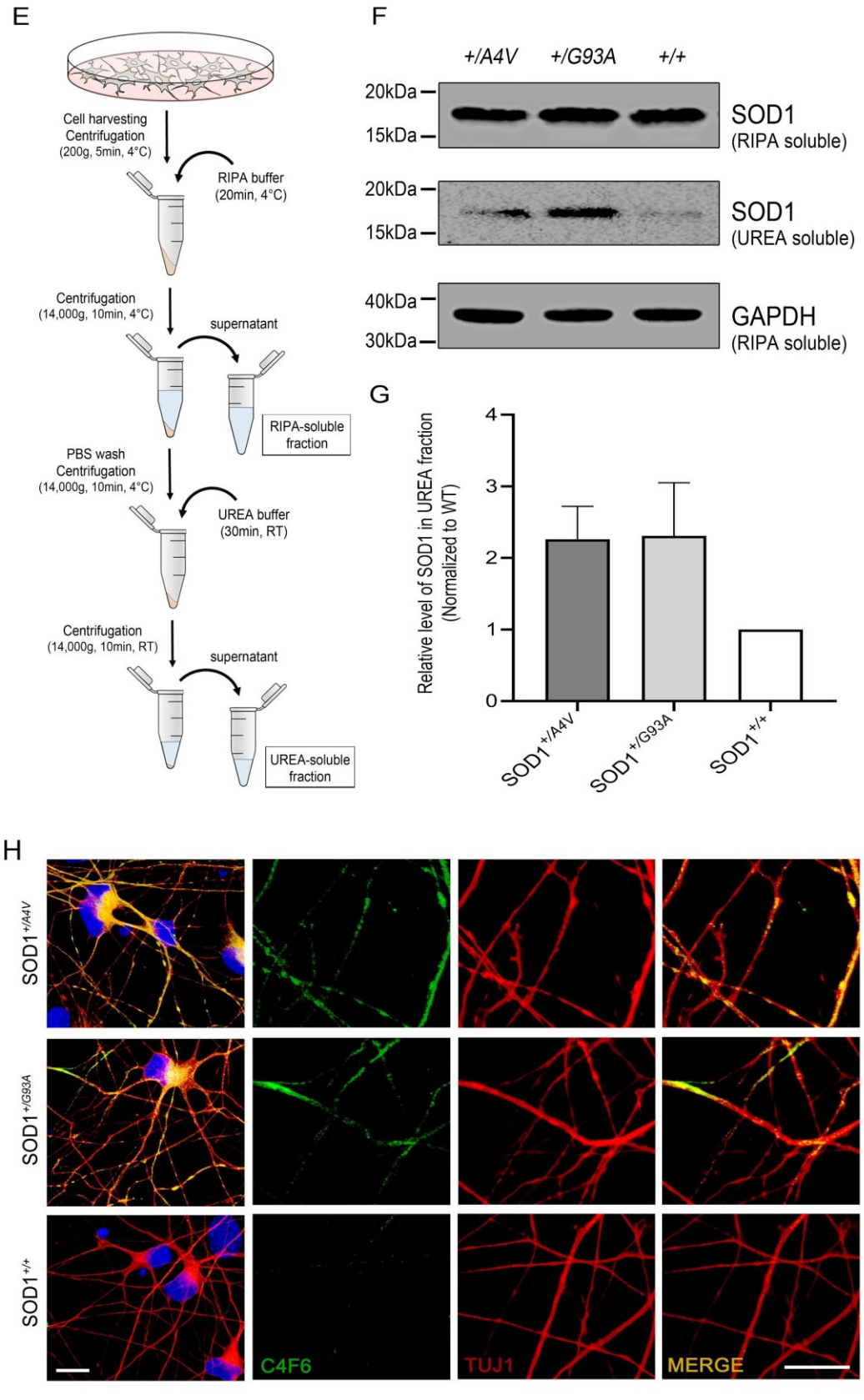
E
Cell harvesting
Centrifugation
(200g, 5min, 4°C)
RIPA buffer
(20min, 4°C)
Centrifugation
(14,000g, 10min, 4°C)
supernatant
RIPA-soluble fraction
PBS wash
Centrifugation
(14,000g, 10min, 4°C)
UREA buffer
(30min, RT)
Centrifugation
(14,000g, 10min, RT)
supernatant
UREA-soluble fraction
F
+/A4V
+/G93A
+/+
20kDa
15kDa
SOD1
(RIPA soluble)
20kDa
15kDa
SOD1
(UREA soluble)
40kDa
30kDa
GAPDH
(RIPA soluble)
G
Relative level of SOD1 in UREA fraction
(Normalized to WT)
0
1
2
3
4
SOD1+/A4V
SOD1+/G93A
SOD1+/+
H
SOD1+/A4V
SOD1+/G93A
SOD1+/+
C4F6
TUJ1
MERGE

Mutant motor neurons showed axonal pathologies and cell body attrition.

As misfolded and aggregated SOD1 in motor neuron processes including axons were observed, we examined if there is any axonal pathology, which is a key feature of ALS, occurring in the mutant lines (Carpenter, 1968; Delisle & Carpenter, 1984; Fischer et al., 2004; Hirano et al., 1984). In order for motor neurons to build a neuronal network and communicate with each other, they need to elongate the axon and multiple dendrites. Aberrant elongation and branching of processes and axonal truncations could result in neurodegeneration, leading to cell death (Delisle & Carpenter, 1984; Fischer & Glass, 2007). Therefore, we measured axonal length 2, 4, and 6 days after plating individual motor neurons on day 18 and compared the mutants to the wild-type. Two days postplating, motor neurons did not present any difference in axonal length. However, the axonal length in the mutants were significantly shorter on 4d and 6d postplating (Fig. 5A and 5B). Moreover, defects in axonal branching were observed. Motor neurons with A4V-SOD1 and G93A-SOD1 mutations had less number of axonal branch points when compared to the wild-type (Fig. 5C and 5D). Another pathological feature, which precedes neuronal apoptosis, we found was axonal swelling (Delisle & Carpenter, 1984). SOD1 mutant motor neurons displayed focal enlargement in their axons with a beaded or fragmented morphology (Fig. 5E). In addition to axonal pathology, cell body attrition was observed. Motor neurons carrying the mutations showed 20-25% reduction in soma size when compared to the wild-type (Fig. 6F and 6G).

Figure 5. Axonal pathology in SOD1$^{+/A4V}$ and SOD1$^{+/G93A}$ motor neurons.

(A) Representative images of motor neurons showing different axonal lengths. Scale bar, 20 μm. (B) Quantification of average axonal length. n = minimum of 16 cells per well with a total of 644

cells with SOD1$^{+/A4V}$ mutation, 523 cells with SOD1$^{+/G93A}$ mutation, and 569 cells with SOD1$^{+/+}$ from 4 wells for each time point. (C) Representative images of neurite tracing. Numbers in red indicate axonal branch points in each line. (D) Quantification of dendritic and axonal branch points. n = minimum of 17 cells per well with a total of 258 cells with SOD1$^{+/A4V}$ mutation, 186 cells with SOD1$^{+/G93A}$ mutation, and 176 cells with SOD1$^{+/+}$ from 4 wells each. All data shown as mean ± SEM. *p < 0.05, **p < 0.01.

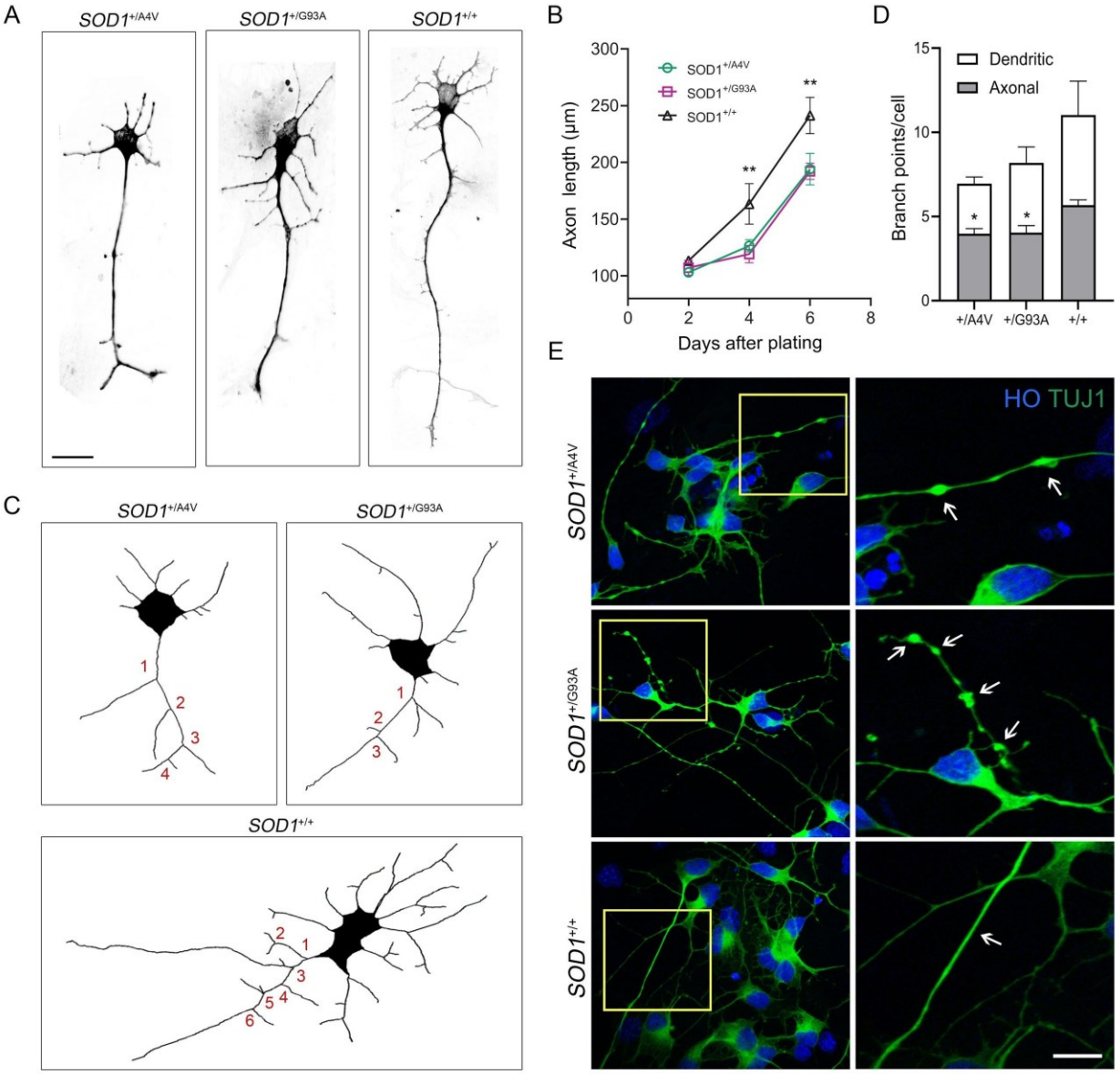

Figure 6. Cell body attrition in SOD1$^{+/A4V}$ and SOD1$^{+/G93A}$ motor neurons.

(A) Immunofluorescence images of TUJ1^{+} motor neurons showing different soma sizes. Scale bar, 10 µm. (B) Quantification of soma size. n = minimum of 25 cells per well with a total of 315 cells with SOD1$^{+/A4V}$ mutation, 206 cells with SOD1$^{+/G93A}$ mutation, and 266 cells with SOD1$^{+/+}$ from 4 wells each. All data shown as mean ± SEM. **P < 0.01.

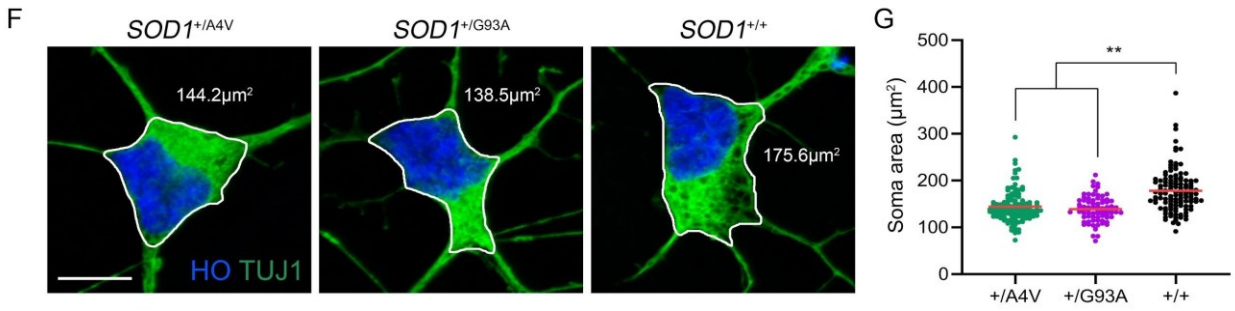

Mutant motor neurons exhibited larger postsynaptic puncta size and more numbers of synapses.

Synaptic dysregulation has been studied as an early pathological event contributing to motor deficits in ALS. Consequently, along with the distal axon, synapse has been receiving great attention as a promising target for the disease (Cantor et al., 2018; Casas, Manzano, Vaz, Osta, & Brites, 2016; Murray et al., 2010; van Zundert, Izaurieta, Fritz, & Alvarez, 2012). We looked for synaptopathy in the mutant iPSC-derived motor neurons by performing immunofluorescence staining (Fig. 7A) and observed some interesting results regarding synapse size and density, both of which are known to be highly associated with the disease progression (Sasaki & Maruyama, 1994; Shiihashi et al., 2017; Starr & Sattler, 2018). When measuring the size of presynaptic puncta immunolabeled by synapsin, the results were not consistent between the two mutants; the average puncta size of SOD1$^{+/A4V}$ motor neurons was smaller than the wild-type whereas that of SOD1$^{+/G93A}$ motor neurons was larger (Fig. 7B). For the size of postsynaptic puncta labeled by PSD95, however, both SOD1$^{+/A4V}$ and SOD1$^{+/G93A}$ motor neurons showed significantly larger

puncta size than the wild-type (Fig. 7C). The synaptic puncta density (number of puncta per 100µm), was also quantified. Although statistically not significant in general, the pre- and postsynaptic puncta densities were relatively higher in both mutants compared to the control wild-type (Fig. 7D and 7E). We also carefully examined the density of synapses, sites at which both synapsin and PSD95 are colocalized. More numbers of $SYN^{+}PSD95^{+}$ puncta per 100 µm were found in the mutants and the difference was statistically significant (Fig. 7F).

Figure 7. Synaptic dysregulation in $SOD1^{+/A4V}$ and $SOD1^{+/G93A}$ motor neurons.

(A) Immunofluorescence images of SYN^{+} and $PSD95^{+}$ motor neurons showing pre- and postsynaptic puncta. Scale bar, 10 µm. (B-C) Quantification of (B) SYN^{+} and (C) $PSD95^{+}$ puncta sizes. (D-F) Quantification of (D) SYN^{+}, (E) $PSD95^{+}$, and (F) $SYN^{+}PSD95^{+}$ puncta density (per 100 µm). Each dot indicates a dendrite analyzed. All data shown as mean ± SEM. *p < 0.05.

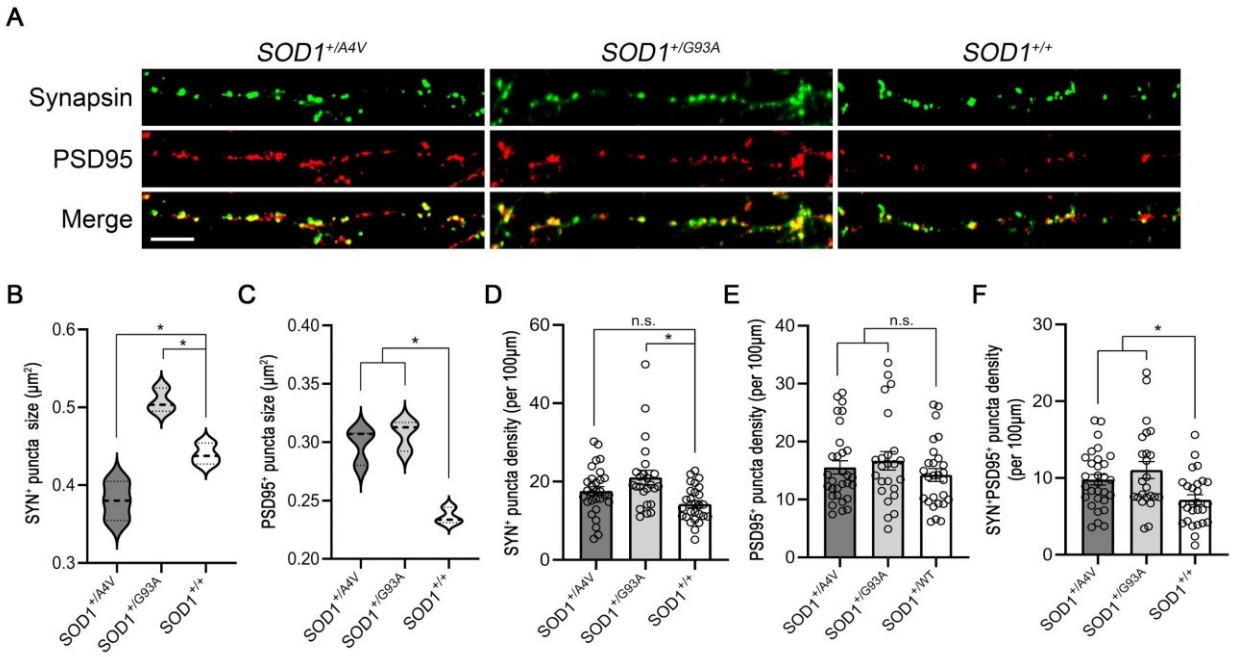

Discussion

We have identified ALS-relevant disease phenotypes with genome-edited iPSC-derived motor neurons with G93A-SOD1 and the results were prominent when compared to its isogenic wildtype control and similar to a positive control having A4V-SOD1 mutation. We first examined the possible presence of misfolded and aggregated SOD1 in motor neurons, which is a pathological hallmark of ALS (Pare et al., 2018). To demonstrate whether the mutant motor neurons produce misfolded SOD1, we used a well-characterized antibody raised against recombinant apo G93A-SOD1, clone C4F6, and stained motor neurons (Urushitani, Ezzi, & Julien, 2007). This antibody has been shown to recognize misfolded forms of mutant human SOD1 proteins including G93A-, A4V-, and the wildtype SOD1 (Atlasi et al., 2018; Pare et al., 2018; Pickles et al., 2016; Rotunno et al., 2014; Xu et al., 2015). As seen in Fig. 4A, 4B, and 4H, 20-30% of mutant motor neurons showed immunoreactivity to the antibody with 10% having SOD1 inclusions. Wildtype motor neurons, although the amount of misfolded, insoluble form was significantly less than the mutants (Fig. 4E, 4F, and 4G), did show some positive signals with the antibody (Fig. 4C and 4D), supporting the hypothesis proposed by previous studies that familial ALS and sporadic ALS share some common pathways and mechanisms (Pare et al., 2018). More interestingly, these misfolded and aggregated SOD1 proteins were localized not only in soma but also in the processes such as dendrites and axons (Fig. 4H). This result led us to investigate axonopathy that could be present in the motor neurons.

We first compared the axonal outgrowth of motor neurons and found pathology in the mutants. When measuring the length of the axon, identified as TAU-positive but MAP2-negative neurite, we showed a reduction of the axonal lengths by 20-30% in G93A-SOD1 and A4V-SOD1 motor neurons 4d and 6d after plating. The number of branch points in the axons of the

mutants also decreased by similar extent (Fig. 5C and 5D). Moreover, bead-like swellings along the axons of the motor neurons with SOD1 mutations were seen (Fig. 5E).

These misfolded, aggregated SOD1 and some axonal pathologies that we observed in the mutants are meaningful as they might be related to the deficits in intracellular trafficking, which are one of the pathological events in ALS. Previous studies have suggested that misfolded SOD1 disrupts ER-to-Golgi trafficking driven by COPII vesicles (Burk & Pasterkamp, 2019). Also, it has been shown that the mutant SOD1 inhibits kinesin- and dynein-mediated axonal transport (Huai & Zhang, 2019). As axonal transport is an essential cellular process responsible for the movement of molecular cargos including lipids, mitochondria, proteins, and cellular organelles in neurons (Burk & Pasterkamp, 2019), its defect has been suggested as the pathogenesis of the disease. The impairment of the transport system has been demonstrated to increase stalling of cellular cargos along the axon, resulting in axonal swelling (Fassier et al., 2013).

The aberrant axonal branching shown in this study is another important ALS pathology that may have disadvantage in neuronal network formation and signal transmission (Suzuki, Akiyama, Warita, & Aoki, 2020). Shorter axonal length and poor branching in the mutants could prevent or minimize neurons from extending multiple branches and arborizing at specific targets (Kalil & Dent, 2014). Motor neurons, in particular, elongate their terminal arbors to muscle fibers and form neuromuscular junctions (NMJs) for muscle contraction. As dismantling of NMJs is known to play a critical role in the onset of ALS (Cappello & Francolini, 2017), rescuing these disease phenotypes in the mutant motor neurons would be worthwhile.

Dysregulation of synapses has long been thought to play a role in many neurodegenerative diseases including ALS from a number of different studies. Here, we compared 60d-old, mature motor neurons and found some distinctive patterns in the mutants regarding synapses. The first

notable observation that the mutant motor neurons showed larger postsynaptic puncta size demonstrated by postsynapse staining with a PSD95 antibody was unexpected and also surprising. PSD95 is a major member of the membrane-associated guanylate kinase family and known for regulating glutamate receptors in the synapse. More importantly, the size and intensity of PSD95 puncta have been shown to correlate with synaptic development and maturity of excitatory synapses (El-Husseini, Schnell, Chetkovich, Nicoll, & Bredt, 2000). In iPSC-derived motor neurons from C9ORF72 ALS/FTD patients, cell surface levels of NMDA receptor NR1 and the AMPA receptor GluR1 were increased and these glutamate receptors were accumulated at postsynaptic densities (PSD, defined as protein dense area in the postsynaptic compartment) (Shi et al., 2018). Overexpression of TDP-43^{A315T} in mouse cortical neurons also showed elevated levels of GluR1 (Jiang et al., 2019).

We have also found that $SYN^{+}PSD95^{+}$synaptic puncta density was higher in the mutants. This corresponds to the results acquired by Fogarty et al. in which excitatory synaptic inputs and dendritic spine densities were increased in presymptomatic TDP-43^{Q331K} mice, proposing excitatory neurotransmission as a pathophysiology of ALS, consistent with the concept of excitotoxicity (Fogarty et al., 2016). One of FDA drugs for treating ALS, riluzole, purportedly acts by blocking excitotoxicity, though no disease-modifying effects are seen. Relevant studies on iPSC-derived MNs with SOD1 mutations have also been done. Although a contradicting result, hypoexcitability of mutant iPSC-derived MNs with SOD1-D90A and SOD1-R115G mutations, exists (Naujock et al., 2016) (Naujock et al., 2016), Wainger et al. demonstrated intrinsic hyperexcitability of iPSC-derived MNs with SOD1-A4V mutation and showed reduced delayed-rectifier potassium currents as a driver (Wainger et al., 2014), which supports the idea of excitotoxicity as a mechanism of the disease (Vasques, Mendez-Otero, & Gubert, 2020).

Combining these previous findings, our results on synaptic dysregulation suggest that mutant SOD1 motor neurons exhibit more advanced maturation of synapses, with abnormal development of postsynapses playing a crucial role, and this could be linked to an earlier cellular and molecular mechanism of ALS.

Chapter 5. Conclusions

This study demonstrated that an iPSC line harboring a heterozygous G93A-SOD1 mutation, which was generated by CRISPR/Cas9 genome editing system, was differentiated into highly pure spinal motor neurons and exhibited ALS-relevant disease phenotypes.

Much studies have been done using genome editing systems on iPSCs but they are mostly focused on genetic correction of a mutation to the wildtype. Observation of rescued phenotypes after genetic correction is worthwhile for determining the possible clinical application of genome editing, including CRISPR/Cas9 system, to humans. However, generating an iPSC line with a disease-causing mutation from its endogenous wildtype gene and confirming the disease-related phenotypes is another way of validating the genome editing system and could be a valuable approach to study the disease mechanism. In particular, an iPSC expressing G93A-SOD1 mutation has never been generated before. This is especially important as the G93A variant is one of the highly studied mutations in ALS and known to have relatively rapid disease progression. Thus, our novel cell line is very suitable for ALS research (Pansarasa et al., 2018). Also, it can be a good comparison to the G93A-SOD1 Transgenic (Tg) mouse or rat, a most widely used and characterized rodent model of ALS. Extensive research on ALS pathogenesis using the Tg-mice has been done for decades but translating the findings from this model to clinical practices has not been successful in general. A possible explanation for this failure is the high copy numbers of human G93A-SOD1 expressed in non-human animals. From this aspect, our iPS cell model, which expresses G93A-SOD1 mutation at physiological level under human genetic background, is a new and alternative tool which can compensate for the current limitations of Tg-mice.

Our findings with the iPSC-derived motor neurons have several meaningful implications. First, we biochemically extracted detergent-insoluble mutant SOD1 from iPSC-derived motor neurons and showed its presence under basal culture condition (Fig. 4E, 4F, and 4G). This result contradicts a previous study that insoluble SOD1 protein was only found when treating iPSC-derived motor neurons with MG132 proteasome inhibitor (Kiskinis et al., 2014) and supports the idea that misfolding and aggregation of SOD1 is a spontaneous pathological hallmark and a possible driver of the disease intrinsic to proteasome dysfunction.

Another ALS-relevant disease phenotype that we found was axonal pathology. We found several spontaneously occurring disease indicators related to axonopathy. For human iPSC-derived G93A-SOD1 harboring motor neurons, these findings are novel and robust. Mutant motor neurons exhibited shorter axonal length, less number of branch points, and axonal swelling. A related trend of having axonal defects, including the number of primary branches, growth cone area, and neurite length, in iPSC-derived neurons have been demonstrated in previous studies on ALS with a different mutation (Groen et al., 2013) or on different motor neuron diseases such as hereditary spastic paraplegias (Havlicek et al., 2014; Rehbach et al., 2019). On the other hand, a recent study on SOD1-G93A Tg mouse model showed enhanced axonal outgrowth and neurite branching in adult motor neurons, as opposed to our data (Osking et al., 2019). However, culture of adult mammalian spinal cord motor neurons is technically challenging and survival and growth is very limited. The discrepancy may be due to variation between the species but may also stem from different stages of disease progression or functional age and viability of cells. Although comparison between the maturity of iPSC-derived spinal motor neurons in cell culture and that of spinal motor neurons *in vivo* have not been clearly addressed, there is a study suggesting that iPSC-derived motor neurons *in vitro* resemble fetal

spinal tissues more than adult spinal tissues when their transcriptomes were analyzed (Ho et al., 2016). However, these results might be highly dependent on densities of the cells in culture and their electrophysiological activities. One might argue that maturation and aging of iPSC-derived motor neurons is needed for better modeling. However, this could be advantageous as the disease phenotypes observed from iPSC-derived motor neurons may reflect early pathology of the disease hence, the results may be better suitable for disease-modifying clinical application.

Excitotoxicity is an enduring proposed mechanism of ALS pathogenesis (Rothstein, 1995; Van Damme, Dewil, Robberecht, & Van Den Bosch, 2005). The larger postsynaptic puncta size and higher synaptic density in the mutant motor neurons could imply enhanced excitatory neurotransmission which could potentially lead to excitotoxicity of neurons. It could also be a compensatory response of the mutant motor neurons having aberrant axonal elongation and branching, and the potential need to augmented excitatory drive. Excitotoxicity is mediated by glutamate receptors and their biology is extraordinarily complex (Dingledine, Borges, Bowie, & Traynelis, 1999). Many species differences are also being discovered in the function and diversity of glutamate receptors (Mayer, 2020). Further investigation is needed to find the linkage between the synaptic dysregulations and excitotoxicity in human motor neurons.

Another notable observation was presynaptic puncta size discrepancy between the two mutants; presynaptic puncta size of A4V-SOD1 motor neurons was smaller than the wildtype and that of G93A-SOD1 motor neurons was larger, with the size of A4V-SOD1 being close to 40% smaller than G93A-SOD1 motor neurons. This suggests that even though the two mutations are within the SOD1 gene locus, different mutations could have discrete mechanisms or at least display different magnitudes or severities in the development of the disease. A variant of this idea has been articulated before because the same gene mutation can cause different disease

phenotypes (Kammenga, 2017) and the general interpretation is that the genetic background and presence of genetic modifiers are playing a significant role in disease development.

In conclusion, the identification of ALS-relevant disease phenotypes in genome-edited, iPSC-derived motor neurons with G93A heterozygous mutation reveals that this cell line was verified as an unprecedented human disease model and can be used to study underlying mechanisms of ALS pathogenesis, which could contribute to the development of therapeutics.

References

Amoroso, M. W., Croft, G. F., Williams, D. J., O'Keeffe, S., Carrasco, M. A., Davis, A. R., . . . Wichterle, H. (2013). Accelerated high-yield generation of limb-innervating motor neurons from human stem cells. *J Neurosci, 33*(2), 574-586. doi:10.1523/JNEUROSCI.0906-12.2013

Atlasi, R. S., Malik, R., Corrales, C. I., Tzeplaeff, L., Whitelegge, J. P., Cashman, N. R., & Bitan, G. (2018). Investigation of Anti-SOD1 Antibodies Yields New Structural Insight into SOD1 Misfolding and Surprising Behavior of the Antibodies Themselves. *ACS Chem Biol, 13*(9), 2794-2807. doi:10.1021/acschembio.8b00729

Bhinge, A., Namboori, S. C., Zhang, X., VanDongen, A. M. J., & Stanton, L. W. (2017). Genetic Correction of SOD1 Mutant iPSCs Reveals ERK and JNK Activated AP1 as a Driver of Neurodegeneration in Amyotrophic Lateral Sclerosis. *Stem Cell Reports, 8*(4), 856-869. doi:10.1016/j.stemcr.2017.02.019

Boillee, S., Yamanaka, K., Lobsiger, C. S., Copeland, N. G., Jenkins, N. A., Kassiotis, G., . . . Cleveland, D. W. (2006). Onset and progression in inherited ALS determined by motor neurons and microglia. *Science, 312*(5778), 1389-1392. doi:10.1126/science.1123511

Boylan, K. (2015). Familial Amyotrophic Lateral Sclerosis. *Neurol Clin, 33*(4), 807-830. doi:10.1016/j.ncl.2015.07.001

Burk, K., & Pasterkamp, R. J. (2019). Disrupted neuronal trafficking in amyotrophic lateral sclerosis. *Acta Neuropathol, 137*(6), 859-877. doi:10.1007/s00401-019-01964-7

Burrows, C. K., Banovich, N. E., Pavlovic, B. J., Patterson, K., Gallego Romero, I., Pritchard, J. K., & Gilad, Y. (2016). Genetic Variation, Not Cell Type of Origin, Underlies the

Majority of Identifiable Regulatory Differences in iPSCs. *PLoS Genet, 12*(1), e1005793. doi:10.1371/journal.pgen.1005793

Calder, E. L., Tchieu, J., Steinbeck, J. A., Tu, E., Keros, S., Ying, S. W., . . . Studer, L. (2015). Retinoic Acid-Mediated Regulation of GLI3 Enables Efficient Motoneuron Derivation from Human ESCs in the Absence of Extrinsic SHH Activation. *J Neurosci, 35*(33), 11462-11481. doi:10.1523/JNEUROSCI.3046-14.2015

Cantor, S., Zhang, W., Delestree, N., Remedio, L., Mentis, G. Z., & Burden, S. J. (2018). Preserving neuromuscular synapses in ALS by stimulating MuSK with a therapeutic agonist antibody. *Elife, 7*. doi:10.7554/eLife.34375

Cappello, V., & Francolini, M. (2017). Neuromuscular Junction Dismantling in Amyotrophic Lateral Sclerosis. *Int J Mol Sci, 18*(10). doi:10.3390/ijms18102092

Carpenter, S. (1968). Proximal axonal enlargement in motor neuron disease. *Neurology, 18*(9), 841-851. doi:10.1212/wnl.18.9.841

Casas, C., Manzano, R., Vaz, R., Osta, R., & Brites, D. (2016). Synaptic Failure: Focus in an Integrative View of ALS. *Brain Plast, 1*(2), 159-175. doi:10.3233/BPL-140001

Chen, H., Qian, K., Du, Z., Cao, J., Petersen, A., Liu, H., . . . Zhang, S. C. (2014). Modeling ALS with iPSCs reveals that mutant SOD1 misregulates neurofilament balance in motor neurons. *Cell Stem Cell, 14*(6), 796-809. doi:10.1016/j.stem.2014.02.004

Chestkov, I. V., Vasilieva, E. A., Illarioshkin, S. N., Lagarkova, M. A., & Kiselev, S. L. (2014). Patient-Specific Induced Pluripotent Stem Cells for SOD1-Associated Amyotrophic Lateral Sclerosis Pathogenesis Studies. *Acta Naturae, 6*(1), 54-60. Retrieved from https://www.ncbi.nlm.nih.gov/pubmed/24772327

Cradick, T. J., Qiu, P., Lee, C. M., Fine, E. J., & Bao, G. (2014). COSMID: A Web-based Tool for Identifying and Validating CRISPR/Cas Off-target Sites. *Mol Ther Nucleic Acids, 3*, e214. doi:10.1038/mtna.2014.64

Cruz, M. P. (2018). Edaravone (Radicava): A Novel Neuroprotective Agent for the Treatment of Amyotrophic Lateral Sclerosis. *P T, 43*(1), 25-28. Retrieved from https://www.ncbi.nlm.nih.gov/pubmed/29290672

Delisle, M. B., & Carpenter, S. (1984). Neurofibrillary axonal swellings and amyotrophic lateral sclerosis. *J Neurol Sci, 63*(2), 241-250. doi:10.1016/0022-510x(84)90199-0

Di Giorgio, F. P., Boulting, G. L., Bobrowicz, S., & Eggan, K. C. (2008). Human embryonic stem cell-derived motor neurons are sensitive to the toxic effect of glial cells carrying an ALS-causing mutation. *Cell Stem Cell, 3*(6), 637-648. doi:10.1016/j.stem.2008.09.017

Dingledine, R., Borges, K., Bowie, D., & Traynelis, S. F. (1999). The glutamate receptor ion channels. *Pharmacol Rev, 51*(1), 7-61. Retrieved from https://www.ncbi.nlm.nih.gov/pubmed/10049997

Du, Z. W., Chen, H., Liu, H., Lu, J., Qian, K., Huang, C. L., . . . Zhang, S. C. (2015). Generation and expansion of highly pure motor neuron progenitors from human pluripotent stem cells. *Nat Commun, 6*, 6626. doi:10.1038/ncomms7626

El-Husseini, A. E., Schnell, E., Chetkovich, D. M., Nicoll, R. A., & Bredt, D. S. (2000). PSD-95 involvement in maturation of excitatory synapses. *Science, 290*(5495), 1364-1368. Retrieved from https://www.ncbi.nlm.nih.gov/pubmed/11082065

Elam, J. S., Taylor, A. B., Strange, R., Antonyuk, S., Doucette, P. A., Rodriguez, J. A., . . . Hart, P. J. (2003). Amyloid-like filaments and water-filled nanotubes formed by SOD1 mutant proteins linked to familial ALS. *Nat Struct Biol, 10*(6), 461-467. doi:10.1038/nsb935

Fang, T., Al Khleifat, A., Meurgey, J. H., Jones, A., Leigh, P. N., Bensimon, G., & Al-Chalabi, A. (2018). Stage at which riluzole treatment prolongs survival in patients with amyotrophic lateral sclerosis: a retrospective analysis of data from a dose-ranging study. *Lancet Neurol, 17*(5), 416-422. doi:10.1016/s1474-4422(18)30054-1

Fassier, C., Tarrade, A., Peris, L., Courageot, S., Mailly, P., Dalard, C., . . . Melki, J. (2013). Microtubule-targeting drugs rescue axonal swellings in cortical neurons from spastin knockout mice. *Dis Model Mech, 6*(1), 72-83. doi:10.1242/dmm.008946

Fischer, L. R., Culver, D. G., Tennant, P., Davis, A. A., Wang, M., Castellano-Sanchez, A., . . . Glass, J. D. (2004). Amyotrophic lateral sclerosis is a distal axonopathy: evidence in mice and man. *Exp Neurol, 185*(2), 232-240. doi:10.1016/j.expneurol.2003.10.004

Fischer, L. R., & Glass, J. D. (2007). Axonal degeneration in motor neuron disease. *Neurodegener Dis, 4*(6), 431-442. doi:10.1159/000107704

Fogarty, M. J., Klenowski, P. M., Lee, J. D., Drieberg-Thompson, J. R., Bartlett, S. E., Ngo, S. T., . . . Noakes, P. G. (2016). Cortical synaptic and dendritic spine abnormalities in a presymptomatic TDP-43 model of amyotrophic lateral sclerosis. *Sci Rep, 6*, 37968. doi:10.1038/srep37968

Groen, E. J., Fumoto, K., Blokhuis, A. M., Engelen-Lee, J., Zhou, Y., van den Heuvel, D. M., . . . Pasterkamp, R. J. (2013). ALS-associated mutations in FUS disrupt the axonal distribution and function of SMN. *Hum Mol Genet, 22*(18), 3690-3704. doi:10.1093/hmg/ddt222

Guhr, A., Kobold, S., Seltmann, S., Seiler Wulczyn, A. E. M., Kurtz, A., & Loser, P. (2018). Recent Trends in Research with Human Pluripotent Stem Cells: Impact of Research and

Use of Cell Lines in Experimental Research and Clinical Trials. *Stem Cell Reports, 11*(2), 485-496. doi:10.1016/j.stemcr.2018.06.012

Gurney, M. E., Pu, H., Chiu, A. Y., Dal Canto, M. C., Polchow, C. Y., Alexander, D. D., . . . et al. (1994). Motor neuron degeneration in mice that express a human Cu,Zn superoxide dismutase mutation. *Science, 264*(5166), 1772-1775. doi:10.1126/science.8209258

Havlicek, S., Kohl, Z., Mishra, H. K., Prots, I., Eberhardt, E., Denguir, N., . . . Winner, B. (2014). Gene dosage-dependent rescue of HSP neurite defects in SPG4 patients' neurons. *Hum Mol Genet, 23*(10), 2527-2541. doi:10.1093/hmg/ddt644

Hirano, A., Nakano, I., Kurland, L. T., Mulder, D. W., Holley, P. W., & Saccomanno, G. (1984). Fine structural study of neurofibrillary changes in a family with amyotrophic lateral sclerosis. *J Neuropathol Exp Neurol, 43*(5), 471-480. doi:10.1097/00005072-198409000-00002

Ho, R., Sances, S., Gowing, G., Amoroso, M. W., O'Rourke, J. G., Sahabian, A., . . . Svendsen, C. N. (2016). ALS disrupts spinal motor neuron maturation and aging pathways within gene co-expression networks. *Nat Neurosci, 19*(9), 1256-1267. doi:10.1038/nn.4345

Hsu, P. D., Lander, E. S., & Zhang, F. (2014). Development and applications of CRISPR-Cas9 for genome engineering. *Cell, 157*(6), 1262-1278. doi:10.1016/j.cell.2014.05.010

Huai, J., & Zhang, Z. (2019). Structural Properties and Interaction Partners of Familial ALS-Associated SOD1 Mutants. *Front Neurol, 10*, 527. doi:10.3389/fneur.2019.00527

Imamura, K., Izumi, Y., Watanabe, A., Tsukita, K., Woltjen, K., Yamamoto, T., . . . Inoue, H. (2017). The Src/c-Abl pathway is a potential therapeutic target in amyotrophic lateral sclerosis. *Sci Transl Med, 9*(391). doi:10.1126/scitranslmed.aaf3962

Ionescu, A., & Perlson, E. (2019). Patient-derived co-cultures for studying ALS. *Nat Biomed Eng, 3*(1), 13-14. doi:10.1038/s41551-018-0333-8

Jaarsma, D., Teuling, E., Haasdijk, E. D., De Zeeuw, C. I., & Hoogenraad, C. C. (2008). Neuron-specific expression of mutant superoxide dismutase is sufficient to induce amyotrophic lateral sclerosis in transgenic mice. *J Neurosci, 28*(9), 2075-2088. doi:10.1523/JNEUROSCI.5258-07.2008

Jiang, T., Handley, E., Brizuela, M., Dawkins, E., Lewis, K. E. A., Clark, R. M., . . . Blizzard, C. A. (2019). Amyotrophic lateral sclerosis mutant TDP-43 may cause synaptic dysfunction through altered dendritic spine function. *Dis Model Mech, 12*(5). doi:10.1242/dmm.038109

Johnston, J. A., Dalton, M. J., Gurney, M. E., & Kopito, R. R. (2000). Formation of high molecular weight complexes of mutant Cu, Zn-superoxide dismutase in a mouse model for familial amyotrophic lateral sclerosis. *Proc Natl Acad Sci U S A, 97*(23), 12571-12576. doi:10.1073/pnas.220417997

Kabashi, E., Valdmanis, P. N., Dion, P., & Rouleau, G. A. (2007). Oxidized/misfolded superoxide dismutase-1: the cause of all amyotrophic lateral sclerosis? *Ann Neurol, 62*(6), 553-559. doi:10.1002/ana.21319

Kalil, K., & Dent, E. W. (2014). Branch management: mechanisms of axon branching in the developing vertebrate CNS. *Nat Rev Neurosci, 15*(1), 7-18. doi:10.1038/nrn3650

Kammenga, J. E. (2017). The background puzzle: how identical mutations in the same gene lead to different disease symptoms. *FEBS J, 284*(20), 3362-3373. doi:10.1111/febs.14080

Kawamata, H., & Manfredi, G. (2010). Import, maturation, and function of SOD1 and its copper chaperone CCS in the mitochondrial intermembrane space. *Antioxid Redox Signal, 13*(9), 1375-1384. doi:10.1089/ars.2010.3212

Kiskinis, E., Sandoe, J., Williams, L. A., Boulting, G. L., Moccia, R., Wainger, B. J., . . . Eggan, K. (2014). Pathways disrupted in human ALS motor neurons identified through genetic correction of mutant SOD1. *Cell Stem Cell, 14*(6), 781-795. doi:10.1016/j.stem.2014.03.004

Kosicki, M., Tomberg, K., & Bradley, A. (2018). Repair of double-strand breaks induced by CRISPR-Cas9 leads to large deletions and complex rearrangements. *Nat Biotechnol, 36*(8), 765-771. doi:10.1038/nbt.4192

Le Verche, V., & Przedborski, S. (2010). Is amyotrophic lateral sclerosis a mitochondrial channelopathy? *Neuron, 67*(4), 523-524. doi:10.1016/j.neuron.2010.08.010

Li, H., Yang, Y., Hong, W., Huang, M., Wu, M., & Zhao, X. (2020). Applications of genome editing technology in the targeted therapy of human diseases: mechanisms, advances and prospects. *Signal Transduct Target Ther, 5*, 1. doi:10.1038/s41392-019-0089-y

Li, Y., Balasubramanian, U., Cohen, D., Zhang, P. W., Mosmiller, E., Sattler, R., . . . Rothstein, J. D. (2015). A comprehensive library of familial human amyotrophic lateral sclerosis induced pluripotent stem cells. *PLoS One, 10*(3), e0118266. doi:10.1371/journal.pone.0118266

Liang, X., Potter, J., Kumar, S., Ravinder, N., & Chesnut, J. D. (2017). Enhanced CRISPR/Cas9-mediated precise genome editing by improved design and delivery of gRNA, Cas9 nuclease, and donor DNA. *J Biotechnol, 241*, 136-146. doi:10.1016/j.jbiotec.2016.11.011

Ludolph, A. C., Bendotti, C., Blaugrund, E., Chio, A., Greensmith, L., Loeffler, J. P., . . . von Horsten, S. (2010). Guidelines for preclinical animal research in ALS/MND: A consensus meeting. *Amyotroph Lateral Scler, 11*(1-2), 38-45. doi:10.3109/17482960903545334

Maury, Y., Come, J., Piskorowski, R. A., Salah-Mohellibi, N., Chevaleyre, V., Peschanski, M., . . . Nedelec, S. (2015). Combinatorial analysis of developmental cues efficiently converts human pluripotent stem cells into multiple neuronal subtypes. *Nat Biotechnol, 33*(1), 89-96. doi:10.1038/nbt.3049

Mayer, M. L. (2020). Glutamate receptors from diverse animal species exhibit unexpected structural and functional diversity. *J Physiol*. doi:10.1113/JP279026

Moloney, E. B., de Winter, F., & Verhaagen, J. (2014). ALS as a distal axonopathy: molecular mechanisms affecting neuromuscular junction stability in the presymptomatic stages of the disease. *Front Neurosci, 8*, 252. doi:10.3389/fnins.2014.00252

Morrice, J. R., Gregory-Evans, C. Y., & Shaw, C. A. (2018). Animal models of amyotrophic lateral sclerosis: A comparison of model validity. *Neural Regen Res, 13*(12), 2050-2054. doi:10.4103/1673-5374.241445

Murray, L. M., Talbot, K., & Gillingwater, T. H. (2010). Review: neuromuscular synaptic vulnerability in motor neurone disease: amyotrophic lateral sclerosis and spinal muscular atrophy. *Neuropathol Appl Neurobiol, 36*(2), 133-156. doi:10.1111/j.1365-2990.2010.01061.x

Naujock, M., Stanslowsky, N., Bufler, S., Naumann, M., Reinhardt, P., Sterneckert, J., . . . Petri, S. (2016). 4-Aminopyridine Induced Activity Rescues Hypoexcitable Motor Neurons from Amyotrophic Lateral Sclerosis Patient-Derived Induced Pluripotent Stem Cells. *Stem Cells, 34*(6), 1563-1575. doi:10.1002/stem.2354

Osking, Z., Ayers, J. I., Hildebrandt, R., Skruber, K., Brown, H., Ryu, D., . . . Vitriol, E. A. (2019). ALS-Linked SOD1 Mutants Enhance Neurite Outgrowth and Branching in Adult Motor Neurons. *iScience, 19*, 448-449. doi:10.1016/j.isci.2019.08.004

Pansarasa, O., Bordoni, M., Diamanti, L., Sproviero, D., Gagliardi, S., & Cereda, C. (2018). SOD1 in Amyotrophic Lateral Sclerosis: "Ambivalent" Behavior Connected to the Disease. *Int J Mol Sci, 19*(5). doi:10.3390/ijms19051345

Pare, B., Lehmann, M., Beaudin, M., Nordstrom, U., Saikali, S., Julien, J. P., . . . Gros-Louis, F. (2018). Misfolded SOD1 pathology in sporadic Amyotrophic Lateral Sclerosis. *Sci Rep, 8*(1), 14223. doi:10.1038/s41598-018-31773-z

Petrov, D., Daura, X., & Zagrovic, B. (2016). Effect of Oxidative Damage on the Stability and Dimerization of Superoxide Dismutase 1. *Biophys J, 110*(7), 1499-1509. doi:10.1016/j.bpj.2016.02.037

Philips, T., & Rothstein, J. D. (2015). Rodent Models of Amyotrophic Lateral Sclerosis. *Curr Protoc Pharmacol, 69*, 5 67 61-65 67 21. doi:10.1002/0471141755.ph0567s69

Pickles, S., Semmler, S., Broom, H. R., Destroismaisons, L., Legroux, L., Arbour, N., . . . Vande Velde, C. (2016). ALS-linked misfolded SOD1 species have divergent impacts on mitochondria. *Acta Neuropathol Commun, 4*(1), 43. doi:10.1186/s40478-016-0313-8

Reaume, A. G., Elliott, J. L., Hoffman, E. K., Kowall, N. W., Ferrante, R. J., Siwek, D. F., . . . Snider, W. D. (1996). Motor neurons in Cu/Zn superoxide dismutase-deficient mice develop normally but exhibit enhanced cell death after axonal injury. *Nat Genet, 13*(1), 43-47. doi:10.1038/ng0596-43

Rehbach, K., Kesavan, J., Hauser, S., Ritzenhofen, S., Jungverdorben, J., Schule, R., . . . Brustle, O. (2019). Multiparametric rapid screening of neuronal process pathology for drug target

identification in HSP patient-specific neurons. *Sci Rep, 9*(1), 9615. doi:10.1038/s41598-019-45246-4

Richard, J. P., & Maragakis, N. J. (2015). Induced pluripotent stem cells from ALS patients for disease modeling. *Brain Res, 1607*, 15-25. doi:10.1016/j.brainres.2014.09.017

Rosen, D. R., Siddique, T., Patterson, D., Figlewicz, D. A., Sapp, P., Hentati, A., . . . et al. (1993). Mutations in Cu/Zn superoxide dismutase gene are associated with familial amyotrophic lateral sclerosis. *Nature, 362*(6415), 59-62. doi:10.1038/362059a0

Rothstein, J. D. (1995). Excitotoxic mechanisms in the pathogenesis of amyotrophic lateral sclerosis. *Adv Neurol, 68*, 7-20; discussion 21-27. Retrieved from https://www.ncbi.nlm.nih.gov/pubmed/8787245

Rotunno, M. S., Auclair, J. R., Maniatis, S., Shaffer, S. A., Agar, J., & Bosco, D. A. (2014). Identification of a misfolded region in superoxide dismutase 1 that is exposed in amyotrophic lateral sclerosis. *J Biol Chem, 289*(41), 28527-28538. doi:10.1074/jbc.M114.581801

Rotunno, M. S., & Bosco, D. A. (2013). An emerging role for misfolded wild-type SOD1 in sporadic ALS pathogenesis. *Front Cell Neurosci, 7*, 253. doi:10.3389/fncel.2013.00253

Sasaki, S., & Maruyama, S. (1994). Synapse loss in anterior horn neurons in amyotrophic lateral sclerosis. *Acta Neuropathol, 88*(3), 222-227. doi:10.1007/BF00293397

Schildge, S., Bohrer, C., Beck, K., & Schachtrup, C. (2013). Isolation and culture of mouse cortical astrocytes. *J Vis Exp*(71). doi:10.3791/50079

Seminary, E. R., Sison, S. L., & Ebert, A. D. (2018). Modeling Protein Aggregation and the Heat Shock Response in ALS iPSC-Derived Motor Neurons. *Front Neurosci, 12*, 86. doi:10.3389/fnins.2018.00086

Shi, Y., Lin, S., Staats, K. A., Li, Y., Chang, W. H., Hung, S. T., . . . Ichida, J. K. (2018). Haploinsufficiency leads to neurodegeneration in C9ORF72 ALS/FTD human induced motor neurons. *Nat Med, 24*(3), 313-325. doi:10.1038/nm.4490

Shiihashi, G., Ito, D., Arai, I., Kobayashi, Y., Hayashi, K., Otsuka, S., . . . Suzuki, N. (2017). Dendritic Homeostasis Disruption in a Novel Frontotemporal Dementia Mouse Model Expressing Cytoplasmic Fused in Sarcoma. *EBioMedicine, 24*, 102-115. doi:10.1016/j.ebiom.2017.09.005

Shinder, G. A., Lacourse, M. C., Minotti, S., & Durham, H. D. (2001). Mutant Cu/Zn-superoxide dismutase proteins have altered solubility and interact with heat shock/stress proteins in models of amyotrophic lateral sclerosis. *J Biol Chem, 276*(16), 12791-12796. doi:10.1074/jbc.M010759200

Starr, A., & Sattler, R. (2018). Synaptic dysfunction and altered excitability in C9ORF72 ALS/FTD. *Brain Res, 1693*(Pt A), 98-108. doi:10.1016/j.brainres.2018.02.011

Suzuki, N., Akiyama, T., Warita, H., & Aoki, M. (2020). Omics Approach to Axonal Dysfunction of Motor Neurons in Amyotrophic Lateral Sclerosis (ALS). *Front Neurosci, 14*, 194. doi:10.3389/fnins.2020.00194

Tan, Z. Y., Huang, T., & Ngeow, J. (2018). 65 YEARS OF THE DOUBLE HELIX: The advancements of gene editing and potential application to hereditary cancer. *Endocr Relat Cancer, 25*(8), T141-T158. doi:10.1530/ERC-18-0039

Urushitani, M., Ezzi, S. A., & Julien, J. P. (2007). Therapeutic effects of immunization with mutant superoxide dismutase in mice models of amyotrophic lateral sclerosis. *Proc Natl Acad Sci U S A, 104*(7), 2495-2500. doi:10.1073/pnas.0606201104

Van Damme, P., Dewil, M., Robberecht, W., & Van Den Bosch, L. (2005). Excitotoxicity and amyotrophic lateral sclerosis. *Neurodegener Dis, 2*(3-4), 147-159. doi:10.1159/000089620

van Zundert, B., Izaurieta, P., Fritz, E., & Alvarez, F. J. (2012). Early pathogenesis in the adult-onset neurodegenerative disease amyotrophic lateral sclerosis. *J Cell Biochem, 113*(11), 3301-3312. doi:10.1002/jcb.24234

Vasques, J. F., Mendez-Otero, R., & Gubert, F. (2020). Modeling ALS using iPSCs: is it possible to reproduce the phenotypic variations observed in patients in vitro? *Regen Med, 15*(7), 1919-1933. doi:10.2217/rme-2020-0067

Vigilante, A., Laddach, A., Moens, N., Meleckyte, R., Leha, A., Ghahramani, A., . . . Watt, F. M. (2019). Identifying Extrinsic versus Intrinsic Drivers of Variation in Cell Behavior in Human iPSC Lines from Healthy Donors. *Cell Rep, 26*(8), 2078-2087 e2073. doi:10.1016/j.celrep.2019.01.094

Wainger, B. J., Kiskinis, E., Mellin, C., Wiskow, O., Han, S. S., Sandoe, J., . . . Woolf, C. J. (2014). Intrinsic membrane hyperexcitability of amyotrophic lateral sclerosis patient-derived motor neurons. *Cell Rep, 7*(1), 1-11. doi:10.1016/j.celrep.2014.03.019

Wang, J., Xu, G., & Borchelt, D. R. (2002). High molecular weight complexes of mutant superoxide dismutase 1: age-dependent and tissue-specific accumulation. *Neurobiol Dis, 9*(2), 139-148. doi:10.1006/nbdi.2001.0471

Wang, L., Yi, F., Fu, L., Yang, J., Wang, S., Wang, Z., . . . Liu, G. H. (2017). CRISPR/Cas9-mediated targeted gene correction in amyotrophic lateral sclerosis patient iPSCs. *Protein Cell, 8*(5), 365-378. doi:10.1007/s13238-017-0397-3

Wen, Z., Nguyen, H. N., Guo, Z., Lalli, M. A., Wang, X., Su, Y., . . . Ming, G. L. (2014). Synaptic dysregulation in a human iPS cell model of mental disorders. *Nature, 515*(7527), 414-418. doi:10.1038/nature13716

Wong, P. C., Pardo, C. A., Borchelt, D. R., Lee, M. K., Copeland, N. G., Jenkins, N. A., . . . Price, D. L. (1995). An adverse property of a familial ALS-linked SOD1 mutation causes motor neuron disease characterized by vacuolar degeneration of mitochondria. *Neuron, 14*(6), 1105-1116. doi:10.1016/0896-6273(95)90259-7

Xu, G., Ayers, J. I., Roberts, B. L., Brown, H., Fromholt, S., Green, C., & Borchelt, D. R. (2015). Direct and indirect mechanisms for wild-type SOD1 to enhance the toxicity of mutant SOD1 in bigenic transgenic mice. *Hum Mol Genet, 24*(4), 1019-1035. doi:10.1093/hmg/ddu517

Yamanaka, K., Boillee, S., Roberts, E. A., Garcia, M. L., McAlonis-Downes, M., Mikse, O. R., . . . Goldstein, L. S. (2008). Mutant SOD1 in cell types other than motor neurons and oligodendrocytes accelerates onset of disease in ALS mice. *Proc Natl Acad Sci U S A, 105*(21), 7594-7599. doi:10.1073/pnas.0802556105

Byung Woo Kim

PERSONAL INFORMATION

Laboratory address: Johns Hopkins School of Medicine
720 Rutland Ave.
Ross Research Building, Room 544
Baltimore, MD 21205

Email: bkim64@jhmi.edu
Phone: 405-371-3766

EDUCATION

2013 – Present
Johns Hopkins University, Baltimore, MD
Ph.D. candidate in Pathobiology
Thesis advisor: Dr. Lee J. Martin, Ph.D.

2008 – 2011
University of Oklahoma, Norman, OK
B.S. Biochemistry *with distinction*
Thesis advisor: Dr. Helen I. Zgurskaya, Ph.D.

RESEARCH EXPERIENCE

2013 – Present
Johns Hopkins University, School of Medicine, Baltimore, MD.
Dr. Lee J. Martin's Laboratory, *Graduate Researcher*.
- Disease modeling of amyotrophic lateral sclerosis (ALS) using iPS cells and CRISPR-Cas9 system.
- Investigation of the role of nuclear hSOD1 as a possible novel mechanism in ALS pathogenesis.
- Investigation of calcium channel activity as a probable cause of motor neuron degeneration in amyotrophic lateral sclerosis with hSOD1 mutations.

2010 – 2013
University of Oklahoma, **Department of Chemistry and Biochemistry**, Norman, OK.
Dr. Helen I. Zgurskaya's Laboratory, *Undergraduate Researcher / Research Assistant.*
- Investigation of membrane transport protein Cg0722: Molecular cloning, gene expression, protein purification, and biochemical analyses.

2009
University of Oklahoma, **Department of Chemistry and Biochemistry,** Norman, OK.
Dr. Chuanbin Mao's Laboratory, *Undergraduate Researcher.*
- Applications of phage display in breast cancer model: M13 bacteriophage amplification, purification, isolation of major coat protein, and synthesis of gold nanorods.

PUBLICATION

Kim BW and Martin LJ (2021). "Mending the broken in ALS: DNA damage and repair in motor neuron degeneration." *Neural Regen Res.* 16(1): 104-105.

Kim BW, Ryu JW, Jeong YE, Kim J, Martin LJ (2020, manuscript under review). "Human motor neurons with SOD1-G93A mutation generated from CRISPR/Cas9 gene-edited iPSCs develop pathological features of amyotrophic lateral sclerosis." *Front Cell Neurosci.*

Kim BW*, Jeong YE*, Reed N, Hoke A (2020, manuscript in preparation). "Ethoxyquin prevents somatic and autonomic neuropathy in STZ-induced rat model of type 1 diabetes mellitus." (*Co-first authors)

Kim BW, Jeong YE, Wong M, Martin LJ (2020). "DNA damage accumulates and responses are engaged in human ALS brain and spinal motor neurons and DNA repair is activatable in iPSC-derived motor neurons with SOD1 mutations." *Acta Neuropathol Commun.* 8(1): 7.

Kim S, **Kim BW**, Prizmic VP, Oh E, Yu V, Evans B, Kim D, Garza LA (2019). "Simple Cell Culture Media Expansion of Primary Mouse Keratinocytes." *J Dermatol Sci.* 93(2): 135–138.

PROFESSIONAL MEETINGS & PRESENTATIONS

Kim BW, Ryu JW, Martin LJ (2019, September). "Disease Modeling of Amyotrophic Lateral Sclerosis Using Human iPS Cells and Genome Editing." Oral presentation at the Johns Hopkins Pathobiology Annual Retreat. Baltimore, MD.

Kim BW, Ryu JW, and Marin LJ (2019, June). "Developmental Aspects of Amyotrophic Lateral Sclerosis: Findings in Human Induced Pluripotent Stem Cell-Derived Motor neurons with A4V and G93A Superoxide Dismutase 1 Mutations." Poster presentation at the International Society for Stem Cell Research Annual Meeting. Boston, MA.

Kim BW, Ryu JW, Martin LJ (2018, October). "Standardization of the ChIP Workflow Using Covaris Adaptive Focused Acoustics (AFA) to Study the Transcriptional Regulation of SOD1 in ALS Pathogenesis." Oral presentation at the American Society of Human Genetics Annual Meeting. San Diego, CA.

Kim BW, Ryu JW, Marin LJ (2018, March). "Human Superoxide Dismutase 1 is a Nuclear Protein With Chromatin-Binding Properties: A Possible Novel Mechanism in ALS Pathogenesis." Poster presentation at the Johns Hopkins 20th Annual Department of

Pathology Young Investigator's Day. Baltimore, MD – **Pathology Young Investigator Award for Excellence in Basic Research.**

Kim BW, Kim J, Marin LJ (2017, August). "Generation of Highly Pure and Faithful Spinal Motor Neurons from Human Pluripotent Stem Cells for Amyotrophic Lateral Sclerosis and Spinal Muscular Atrophy Modeling." Poster presentation at the 18th Annual Meeting of Korean-American Scientists and Engineers Association, Washington D.C.

Kim BW, Kim J, Marin LJ (2017, June). "Generation of Highly Pure and Faithful Spinal Motor Neurons from Human Pluripotent Stem Cells for Amyotrophic Lateral Sclerosis and Spinal Muscular Atrophy Modeling." Poster presentation at the International Society for Stem Cell Research Annual Meeting. Boston, MA.

Kim BW and Marin LJ (2016, August). "Voltage-Gated Calcium Channels (VGCCs) and Intracellular Ca^{2+} Dysregulation as Mechanisms of Disease in Amyotrophic Lateral Sclerosis (ALS)." Poster presentation at the 17th Annual Meeting of Korean-American Scientists and Engineers Association, Dallas, TX.

Kim BW and Marin LJ (2014, December). "The Multipotential Neural Stem Cell Line, ReNcell CX, as a Cell Model for Human Neuron Development, Differentiation, and Degeneration." Poster presentation at the 7th Annual Maryland Stem Cell Research Symposium. Maryland Stem Cell Research Fund, Silverspring, MD.

Kim BW and Zgurskaya HI (2012, August). "Cloning, Expression, Purification, and Biochemical Analysis of *Corynebacterium glutamicum cg0722* gene." Poster presentation at the 13th Annual Meeting of Korean-American Scientists and Engineers Association, Los Angeles, CA.

RESEARCH SUPPORT & COLLABORATION

2018

Research support and collaboration with Covaris, Inc.

- Optimized chromatin immunoprecipitation using Covaris Adaptive Focused Acoustics (AFA) to study the transcriptional regulation of SOD1 in ALS pathogenesis.
- Invited to give a talk in the exhibitor session hosted by Covaris, Inc. at the American Society of Human Genetics annual meeting. San Diego, CA.

TEACHING EXPERIENCE

2016 **Johns Hopkins University**, School of Medicine, Baltimore, MD.
Teaching Assistant (Grant Writing Course).

- Taught a session on writing an NIH grant proposal in the format of an NRSA F31 predoctoral training grant proposal.
- Helped to learn and become fully aware of each grant proposal section including specific aims, significance, innovation, and approach.
- Lectured on review process and provided strategies to deal with reviews (pink sheets).

LABORATORY SKILLS

Biochemistry & molecular biology	• Genome editing (CRISPR-Cas9) • Molecular cloning • Gene expression • DNA transformation/transfection • Quantitative-PCR • Site-directed mutagenesis • Chemical cross-linking	• Protein purification (Affinity chromatography) • Chromatin immunoprecipitation • Co-immunoprecipitation • Immunofluorescence staining • TUNEL assay • Western blotting
Cell biology	• Stem cell culture (ESCs, iPSCs) • Neural stem cell differentiation • Motor neuron differentiation	• Mouse primary astrocyte culture • Mammalian cell culture (Human, mouse, rat)
Animal work & Histology	• Mouse breeding • Tissue dissection • Tissue sectioning	• Mouse perfusion • Tissue fractionation • Immunohistochemistry
Microscopy	• Confocal microscopy • Phase-contrast microscopy	• Epifluorescence microscopy • Bright-field microscopy
Software	• Image J • Imaris	• Photoshop • Sigmaplot, GraphPad

HONORS & AWARDS

2018	**Korean Honor Scholarship** Embassy of the Republic of Korea in the USA
2018	**Pathology Young Investigator's Day Award for Excellence in Basic Research** Johns Hopkins University, Baltimore
2017	**UKC 2017 Travel Award** Korean-American Scientists and Engineers Association
2016	**UKC 2016 Travel Award** Korean-American Scientists and Engineers Association
2013	**Margaret Lee Fellowship** Johns Hopkins University, Baltimore, MD
2012	**UKC 2012 Travel Award** Korean-American Scientists and Engineers Association
2011	**Graduation with Distinction** University of Oklahoma, Norman, OK
2011	**Departmental Commencement Banner Carrier for the Outstanding Graduating Student** University of Oklahoma, Norman, OK
2011	**Dean's Honor Roll** University of Oklahoma, Norman, OK

EMPLOYMENT

2013 – Present	**Graduate Student Researcher** Johns Hopkins University, School of Medicine, Baltimore, MD
2012 – 2013	**Research Assistant** University of Oklahoma, Department of Chemistry and Biochemistry, Norman, OK
2005 –2007	**Detox Soldier (Sergeant)** Republic of Korea Army: 13th Chemistry Battalion, Inje, South Korea